

Homologous-recombination-deficient tumours are dependent on Pol0-mediated repair

Raphael Ceccaldi¹, Jessica C. Liu^{1,2,3}, Ravindra Amunugama⁴, Ildiko Hajdu⁵, Benjamin Primack¹, Mark I. R. Petalcorin⁶, Kevin W. O'Connor¹, Panagiotis A. Konstantinopoulos⁷, Stephen J. Elledge⁵, Simon J. Boulton⁶, Timur Yusufzai^{1,2} & Alan D. D'Andrea¹

Large-scale genomic studies have shown that half of epithelial ovarian cancers (EOCs) have alterations in genes regulating homologous recombination (HR) repair¹. Loss of HR accounts for the genomic instability of EOCs and for their cellular hyper-dependence on alternative poly-ADP ribose polymerase (PARP)-mediated DNA repair mechanisms^{2–5}. Previous studies have implicated the DNA polymerase 0 (Pol0 also known as POLQ, encoded by *POLQ*)⁶ in a pathway required for the repair of DNA double-strand breaks^{7–9}, referred to as the error-prone microhomology-mediated end-joining (MMEJ) pathway^{10–13}. Whether Pol0 interacts with canonical DNA repair pathways to prevent genomic instability remains unknown. Here we report an inverse correlation between HR activity and Pol0 expression in EOCs. Knockdown of Pol0 in HR-proficient cells upregulates HR activity and RAD51 nucleofilament assembly, while knockdown of Pol0 in HR-deficient EOCs enhances cell death. Consistent with these results, genetic inactivation of an HR gene (*Fancd2*) and *Polq* in mice results in embryonic lethality. Moreover, Pol0 contains RAD51 binding motifs and it blocks RAD51-mediated recombination. Our results reveal a synthetic lethal relationship between the HR pathway and Pol0-mediated repair in EOCs, and identify Pol0 as a novel druggable target for cancer therapy.

To examine changes in polymerase activity between tumours and normal tissues, we screened polymerase gene expression profiles in a large number of cancers (Supplementary Table 1). Gene set enrichment analysis (GSEA) revealed specific and recurrent overexpression of Pol0 in EOCs (Extended Data Fig. 1a–c). Pol0 was upregulated in a grade-dependent manner and its expression positively correlated with numerous mediators of HR (Extended Data Fig. 1d–j). As Pol0 has been suggested to play a role in DNA repair^{7–10}, we investigated a potential role for Pol0 in HR repair.

To test the relationship between Pol0 expression and HR, we used a cell-based assay in human cells which measures the efficiency of recombination of two GFP alleles (DR-GFP assay)¹⁴. Knockdown of Pol0 with short interfering RNA (siRNA) (Extended Data Fig. 2a) resulted in an increase in HR efficiency, similar to that observed by depleting the anti-recombinases PARI or BLM^{15,16}. Depletion of Pol0 caused a significant increase in basal and radiation (IR)-induced RAD51 foci (Fig. 1a, b and Extended Data Fig. 2b–d), and depletion of Pol0 in 293T cells conferred cellular hypersensitivity to mitomycin C (MMC) and an increase in MMC-induced chromosomal aberrations (Extended Data Fig. 2e, f). These findings suggest that human Pol0 inhibits HR and participates in the maintenance of genome stability.

Given that Pol0 shares structural homology with coexpressed RAD51-binding ATPases (Extended Data Fig. 1k, l), we hypothesized that Pol0 might regulate HR through an interaction with RAD51. RAD51 was detected in Flag-tagged Pol0 immunoprecipitates, and purified full-length

Flag-Pol0 bound recombinant human RAD51 (Fig. 1c, d). Pull-down assays with recombinant GST-RAD51 and *in vitro* translated Pol0 truncation mutants defined a region of Pol0 binding to RAD51 spanning amino acids 847–894 (Fig. 1e, f and Extended Data Fig. 2g, h). Sequence homology of Pol0 with the RAD51 binding domain of *C. elegans* RFS-1 (ref. 17) identified a second binding region (Extended Data Fig. 2i). Peptides arrays narrowed down the RAD51 binding activity of Pol0 to three distinct motifs (Fig. 1g and Extended Data Fig. 2j). Substitution arrays confirmed the interaction and highlighted the importance of the 847–894 Pol0 region as both necessary and sufficient for RAD51 binding (Extended Data Fig. 3a, b). Together these results indicate that Pol0 is a RAD51-interacting protein that regulates HR.

In order to address the role of Pol0 in HR regulation, we assessed the ability of wild-type or mutant Pol0 to complement the siPol0-dependent increase in RAD51 foci. Full-length wild-type Pol0 fully reduced IR-induced RAD51 foci, unlike Pol0 mutated at ATPase catalytic residues (A-dead) or Pol0 lacking interaction with RAD51 (Δ RAD51) (Fig. 2a, b). Expression of a Pol0 mutant lacking the polymerase domain (Δ Pol1) was sufficient to decrease IR-induced RAD51 foci, suggesting that the N-terminal half of Pol0 is sufficient to disrupt RAD51 foci (Fig. 2b and Extended Data Fig. 3c, d). We next measured the ability of wild-type or mutant Pol0 to complement the siPol0-dependent increase in HR efficiency. Again, expression of full-length Pol0 or Δ Pol1 decreased the recombination frequency when compared to cells expressing other Pol0 constructs, suggesting that the N-terminal half of Pol0 containing the RAD51 binding domain and the ATPase domain is needed to inhibit HR (Fig. 2c and Extended Data Fig. 3e).

A purified recombinant Pol0 fragment (Δ Pol2) from insect cells exhibited low levels of basal ATPase activity, as previously reported¹⁸ (Fig. 2d, e). Pol0 ATPase activity was selectively stimulated by the addition of single-stranded DNA (ssDNA) or fork DNA (Fig. 2e and Extended Data Fig. 4a). Electrophoretic mobility gel shift assays (EMSA) showed specific binding of Pol0 to ssDNA (Fig. 2f and Extended Data Fig. 4b). We incubated Δ Pol2 with ssDNA and measured RAD51–ssDNA nucleofilament assembly. Interestingly, RAD51–ssDNA assembly was reduced by Δ Pol2 wild-type but not by A-dead or Δ RAD51, indicating that Pol0 negatively affects RAD51–ssDNA assembly through its RAD51 binding and ATPase activities (Fig. 2g and Extended Data Fig. 4c–f). Furthermore, Pol0 decreased the efficiency of D-loop formation, confirming that Pol0 is a negative regulator of HR (Fig. 2h and Extended Data Fig. 4g–j).

As Pol0 is upregulated in subgroups of cancers associated with HR deficiency (Fig. 3a) and Pol0 activity shows specificity for replicative-stress-mediated structures (ssDNA and fork DNA) (Fig. 2e, f), we examined the cellular functions of Pol0 under replicative stress. Subcellular fractionation revealed that Pol0 is enriched in chromatin in response to ultraviolet (UV) light; and RAD51 binding by Pol0 was enhanced by UV

¹Department of Radiation Oncology, Dana-Farber Cancer Institute, Harvard Medical School, Boston, Massachusetts 02215, USA. ²Department of Biological Chemistry & Molecular Pharmacology, Harvard Medical School, Boston, Massachusetts 02215, USA. ³Department of Molecular & Cellular Biology, Harvard University, Cambridge, Massachusetts 02138, USA. ⁴Howard Hughes Medical Institute, Department of Biological Chemistry and Molecular Pharmacology, Harvard Medical School, Boston, Massachusetts 02215, USA. ⁵Howard Hughes Medical Institute, Division of Genetics, Brigham and Women's Hospital, Boston, Massachusetts 02215, USA. ⁶DNA Damage Response Laboratory, Cancer Research UK, London Research Institute, Clare Hall, South Mimms EN6 3LD, UK. ⁷Department of Medical Oncology, Medical Gynecologic Oncology Program, Dana-Farber Cancer Institute, Harvard Medical School, Boston, Massachusetts 02215, USA.

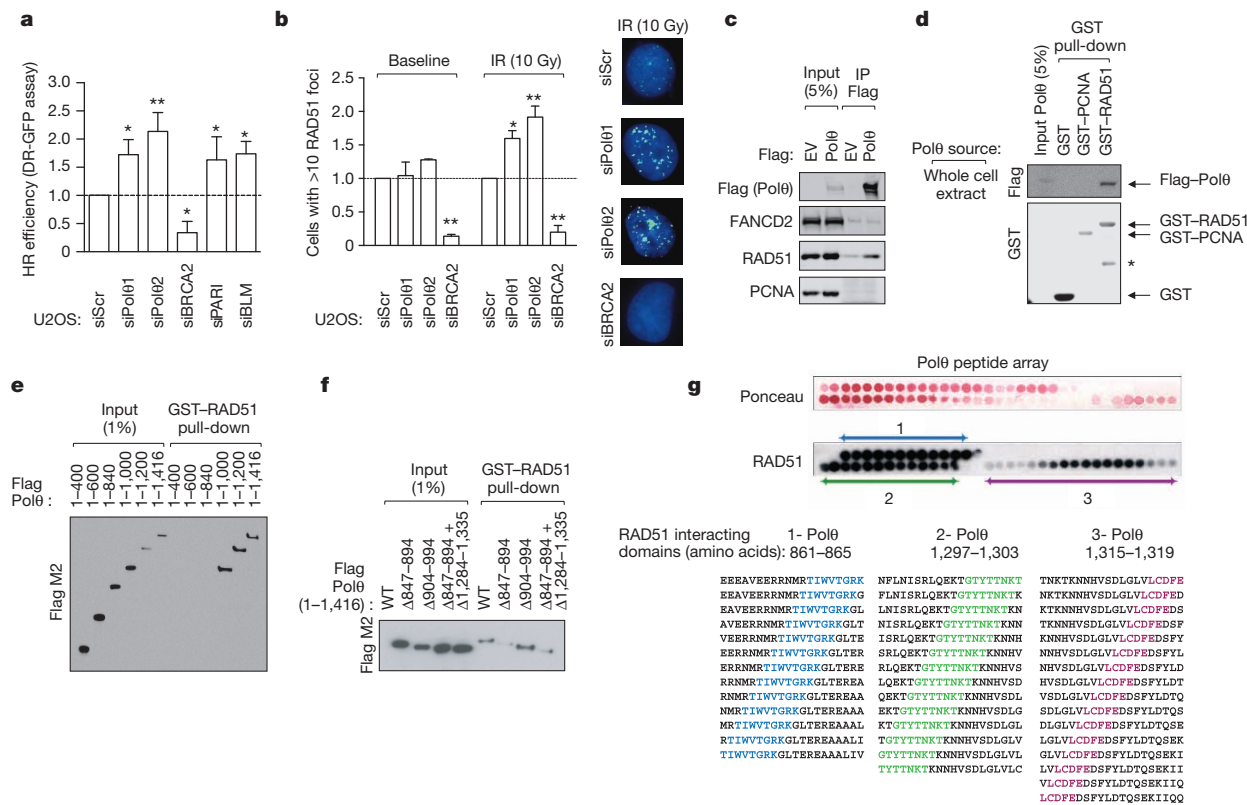


Figure 1 | Polθ is a RAD51-interacting protein that suppresses HR. **a**, DR-GFP assay in U2OS cells transfected with indicated siRNA. **b**, Quantification of RAD51 foci in U2OS cells transfected with indicated siRNA. **c**, Endogenous RAD51 co-precipitates *in vivo* with purified full-length Flag-tagged Polθ from whole cell extracts. EV, empty vector. **d**, GST pull-down experiment with full-length Flag-tagged Polθ (* indicates non-specific band).

exposure, suggesting that Polθ regulates HR in cells under replicative stress (Extended Data Fig. 5a, b). Polθ-depleted cells were hypersensitive to cellular stress and DNA damage, along with an exacerbated checkpoint

e, GST-RAD51 pull-down with *in vitro* translated Polθ truncation mutants. **f**, GST-RAD51 pull-down with *in vitro* translated Polθ versions missing indicated amino acids. **g**, Ponceau staining and immunoblotting of peptide arrays for the indicated Polθ motifs probed with recombinant RAD51. The Polθ amino acids spanning RAD51-interacting motifs are shown. Data in **a** and **b** represent mean \pm s.e.m.

activation and increased γH2AX phosphorylation (Fig. 3b, c). Furthermore, the cell cycle progression of Polθ-depleted cells was impaired after DNA damage (Fig. 3d, e). To determine the role of Polθ in replication

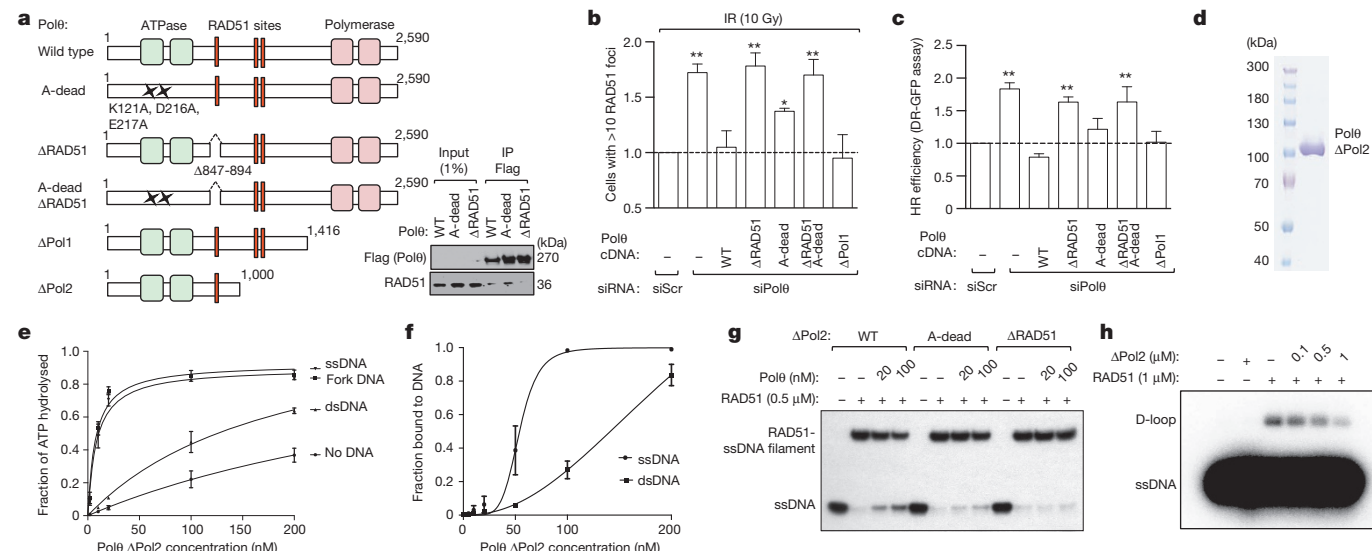


Figure 2 | Polθ inhibits RAD51-mediated recombination. **a**, Schematic of Polθ mutants used in complementation studies and their interaction with RAD51. WT, wild type.

b, Quantification of RAD51 foci in U2OS cells transfected with indicated siRNA and Polθ cDNA constructs refractory to siPolθ1.

c, DR-GFP assay in U2OS cells transfected with indicated siRNA and Polθ cDNA constructs.

d, Coomassie-stained gel of the purified Polθ fragment.

e, Quantification of Polθ ATPase activity.

f, Quantification of Polθ binding to ssDNA and dsDNA.

g, RAD51-ssDNA nucleofilament assembly assay.

h, Assessment of RAD51-dependent D-loop formation.

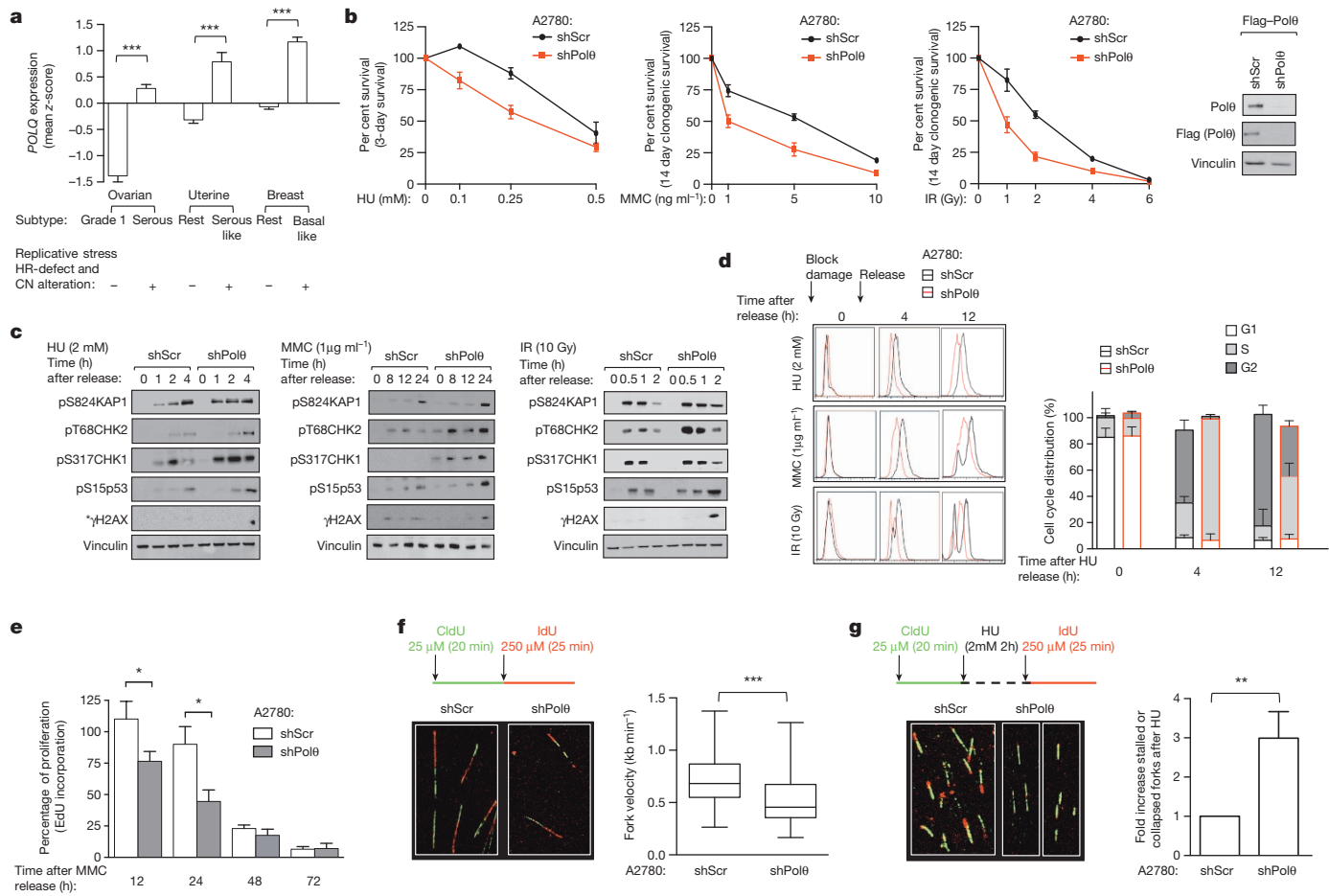


Figure 3 | Pol0 promotes S phase progression and recovery of stalled forks.

a, *POLQ* gene expression in subtypes of cancers with HR deficiency. **b**, Survival assays of A2780 cells exposed to the indicated DNA-damaging agents. Immunoblot showing silencing efficiency is shown on the right. **c**, Immunoblot analyses following pulse treatments with DNA-damaging agents (* γ H2AX: see Methods for specific time points used for γ H2AX immunoblot). HU, hydroxyurea. **d**, Cell cycle progression of synchronized A2780 cells. A

representative cell cycle distribution. **e**, Fraction of cycling A2780 cells measured by 5-ethynyl-2'-deoxyuridine (EdU) incorporation. **f**, Quantification of DNA fibre lengths. **g**, Percentage of stalled forks. All experiments shown in **a–d** were performed in two cell lines (A2780 and 293T). All data represent mean \pm s.e.m., except for box plots in **f** that show twenty-fifth to seventy-fifth percentiles, with lines indicating the median, and whiskers indicating the smallest and largest values.

dynamics, single-molecule analyses were performed on extended DNA fibres¹⁹. Abnormalities in replication fork progression were observed in Pol0-depleted cells (Fig. 3f, g and Extended Data Fig. 5c, d). These results suggest that Pol0 maintains genomic stability at stalled or collapsed replication forks by promoting fork restart.

To examine the regulation of Pol0, we quantified Pol0 expression by RT-qPCR. Pol0 was selectively upregulated in HR-deficient ovarian cancer cell lines. Complementation of BRCA1 or FANCD2-deficient cell lines with BRCA1 and FANCD2 cDNA respectively, restored normal HR function and reduced Pol0 expression to normal levels. Conversely, siRNA-mediated inhibition of HR genes increased Pol0 expression (Extended Data Fig. 5e, f). Pol0 expression was significantly higher in subgroups of cancers with HR deficiency and a high genomic instability pattern²⁰ (Fig. 3a and Extended Data Fig. 5g). Patients with high Pol0 expression had a better response to platinum chemotherapy, a surrogate for HR deficiency, suggesting that Pol0 expression inversely correlates with HR activity and may be useful as a biomarker for platinium sensitivity (Extended Data Fig. 5h, i). Together, these data indicate that increased Pol0 expression is driven by HR deficiency.

To assess the possible synthetic lethality between HR genes and Pol0, we generated an HR-deficient ovarian tumour cell line, A2780-shFANCD2 cells (Extended Data Fig. 6a–c). These cells, and the parental A2780 cells, were subjected to Pol0 depletion, and survival following exposure to cytotoxic drugs was measured. Pol0 depletion reduced the survival of

HR-deficient cells exposed to inhibitors of PARP (PARPi), cisplatin (CDDP) or MMC (Extended Data Fig. 6d–f). Pol0 inhibition impaired the survival of BRCA1-deficient tumours (MDA-MB-436) after PARPi treatment but had no effect on the complemented line (MDA-MB-436 + BRCA1) (Fig. 4a). Pol0-depleted cells were hypersensitive to ATM inhibition, known to create an HR defect phenotype²¹. Chromosomal breakage, checkpoint activation, and γ H2AX phosphorylation in response to MMC were exacerbated by Pol0 depletion (Fig. 4b and Extended Data Fig. 6g, h). Furthermore, a whole-genome short hairpin RNA (shRNA) screen performed on HR-deficient (*FANCA*^{-/-}) fibroblasts showed that shRNAs targeting Pol0 impair cell survival in MMC (Extended Data Fig. 6i), suggesting that HR-deficient cells cannot survive in the absence of Pol0.

Next, we investigated the interaction between the HR and Pol0 pathways *in vivo* by interbreeding *Fancd2*^{+/−} and *Polq*^{+/−} mice. Although *Fancd2*^{−/−} and *Polq*^{−/−} mice are viable and exhibit subtle phenotypes²², viable *Fancd2*^{−/−}*Polq*^{−/−} mice were uncommon from these matings (Extended Data Fig. 7a). The only surviving *Fancd2*^{−/−}*Polq*^{−/−} pups exhibited severe congenital malformations and were either found dead or died prematurely. *Fancd2*^{−/−}*Polq*^{−/−} embryos showed severe congenital malformations, and mouse embryonic fibroblasts (MEFs) generated from *Fancd2*^{−/−}*Polq*^{−/−} embryos showed hypersensitivity to PARPi (Fig. 4c and Extended Data Fig. 7b–e). These data suggest that loss of the HR and Pol0 repair pathways *in vivo* results in embryonic lethality.

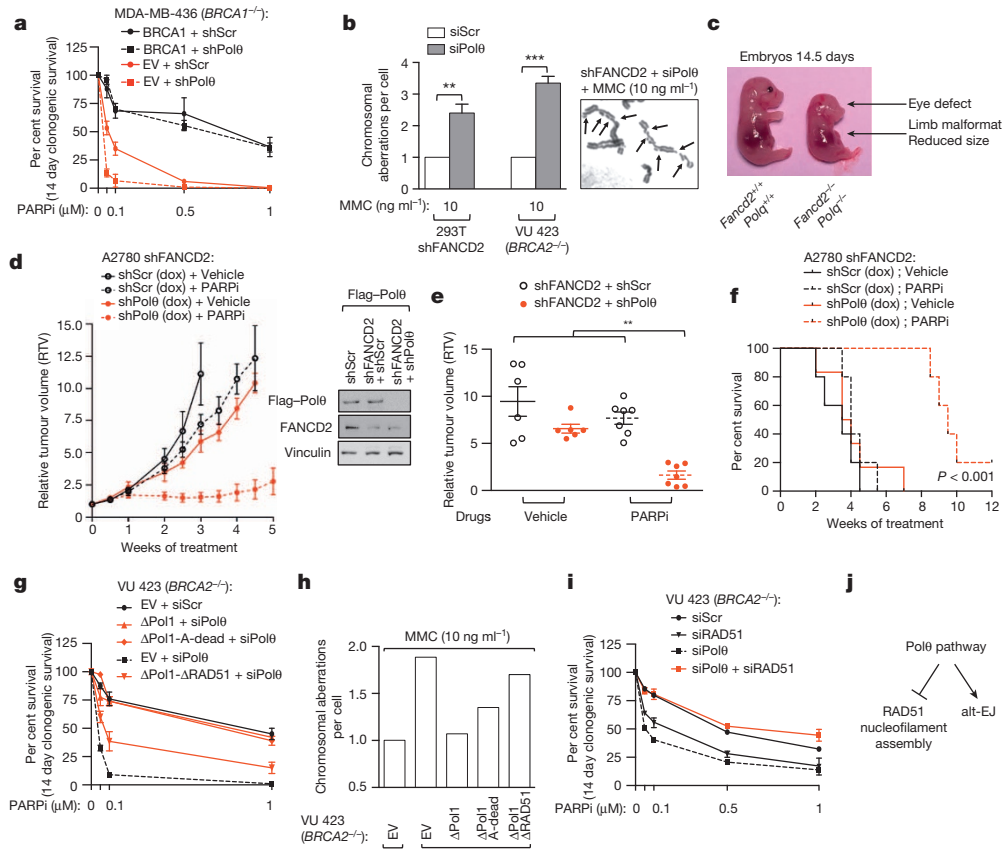


Figure 4 | Synthetic lethality between HR and Pol0 repair pathways. **a**, Clonogenic formation of BRCA1-deficient (MDA-MB-436) cells expressing indicated cDNA together with indicated shRNA. **b**, Chromosome breakage analysis of HR-deficient cells transfected with the indicated siRNA. A representative image is shown. Arrows indicate chromosomal aberrations. **c**, Embryos at day 14 of gestation. **d**, Growth of indicated xenografts *in vivo*. Immunoblot showing silencing efficiency. **e**, Relative tumour volumes (RTV) after three weeks of treatment. **f**, Overall

As xenografts of tumours cells expressing shRNAs against both FANCD2 and Pol0 did not stably propagate in mice (Extended Data Fig. 7f), we xenotransplanted A2780-shFANCD2 cells expressing either doxycycline-inducible Pol0 or scrambled (Scr) shRNA in athymic nude mice. Pol0 depletion significantly impaired tumour growth after PARPi treatment (Fig. 4d, e and Extended Data Fig. 7g, h). Moreover, mice bearing Pol0-depleted tumours had a survival advantage following PARPi treatment compared to control mice (Fig. 4f). Pol0-depleted HR-deficient tumour cells also exhibited decreased survival in *in vivo* dual-colour competition experiments (Extended Data Fig. 7i–l). Collectively, these data confirm that HR-deficient tumours are hypersensitive to inhibition of Pol0-mediated repair.

To understand which functions of Pol0 are required for resistance to DNA-damaging agents, we performed a series of complementation studies in HR-deficient cells. Expression of full-length Pol0 or Δ Pol1, but not Δ RAD51, in HR-deficient Pol0-depleted cells treated with PARPi or MMC was able to rescue toxicity, suggesting that the anti-recombinase activity of Pol0 maintains the genomic stability of HR-deficient cells (Fig. 4g, h and Extended Data Fig. 8a, b). Moreover, the toxicity induced by loss of Pol0 in HR-deficient cells was rescued by depletion of RAD51 showing that, in the absence of Pol0, RAD51 is toxic to HR-deficient cells (Fig. 4i). These results suggest a role for Pol0 in limiting toxic HR events²³ (Extended Data Fig. 8c–f) and may explain why HR-deficient cells overexpress and depend on an anti-recombinase for survival.

High mutation rates have been observed in HR-deficient tumours²⁴. Previous studies have shown that Pol0 is an error-prone polymerase^{25,26}.

survival for mice treated with vehicle or PARPi. Log-rank $P < 10^{-3}$. **g, h**, Clonogenic formation (g) and chromosome breakage analysis (h) of BRCA2-deficient cells expressing Pol0 cDNA constructs refractory to siPol0 and transfected with the indicated siRNA. **i**, Clonogenic formation of BRCA2-deficient cells transfected with the indicated siRNA. **j**, Model for role of Pol0 in DNA repair. Data in **a, b, g** and **i** represent mean \pm s.e.m. For data in **d–f**, each circle represents data from one tumour and each group represents $n \geq 6$ tumours from $n \geq 6$ mice. Brackets show mean \pm s.e.m.

that participates in alternative end-joining (alt-EJ)¹⁰. Therefore, we assessed the role of Pol0 in error-prone DNA repair in human cancer cells. Pol0 inhibition reduced alt-EJ efficiency in U2OS cells, similar to the reduction observed following depletion of PARP1, another critical factor in end-joining^{27,28} (Extended Data Fig. 9a). Expression of full-length Pol0, Δ RAD51, or A-dead, but not the Δ Pol1 mutant, complemented the cells, suggesting that the polymerase domain of Pol0 is required for end-joining (Extended Data Fig. 9b). GFP-tagged full-length Pol0 formed foci after UV treatment in a PARP-dependent manner (Extended Data Fig. 9c). Pol0 inhibition reduced the mutation frequency induced by UV light, and tumours with high Pol0 expression harboured more somatic point mutations than those with lower Pol0 levels (Extended Data Fig. 9d, e). These results suggest that Pol0 contributes to the mutational signature observed in some HR-deficient tumours²⁹.

In human cancers, a deficiency in one DNA repair pathway can result in cellular hyper-dependence on a second compensatory DNA repair pathway⁴. Here we show that Pol0 is overexpressed in EOCs and other tumours with HR defects³⁰. Wild-type Pol0 limits RAD51-ssDNA nucleofilament assembly (Extended Data Fig. 10a) and promotes alt-EJ (Fig. 4j). We demonstrate that HR-deficient tumours are hypersensitive to inhibition of Pol0-mediated repair. Therefore, Pol0 appears to channel DNA repair by antagonizing HR and promoting PARP1-dependent error-prone repair (Extended Data Fig. 10b). These results offer a potential new therapeutic target for cancers with inactivated HR.

Online Content Methods, along with any additional Extended Data display items and Source Data, are available in the online version of the paper; references unique to these sections appear only in the online paper.

Received 1 September; accepted 24 December 2014.

Published online 2 February 2015.

1. The Cancer Genome Atlas Research Network. Integrated genomic analyses of ovarian carcinoma. *Nature* **474**, 609–615 (2011).
2. Farmer, H. *et al.* Targeting the DNA repair defect in BRCA mutant cells as a therapeutic strategy. *Nature* **434**, 917–921 (2005).
3. Bryant, H. E. *et al.* Specific killing of BRCA2-deficient tumours with inhibitors of poly(ADP-ribose) polymerase. *Nature* **434**, 913–917 (2005).
4. Kennedy, R. D. & D'Andrea, A. D. DNA repair pathways in clinical practice: lessons from pediatric cancer susceptibility syndromes. *J. Clin. Oncol.* **24**, 3799–3808 (2006).
5. Bast, R. C. Jr, Hennessy, B. & Mills, G. B. The biology of ovarian cancer: new opportunities for translation. *Nature Rev. Cancer* **9**, 415–428 (2009).
6. Yousefzadeh, M. J. & Wood, R. D. DNA polymerase POLQ and cellular defense against DNA damage. *DNA Repair* **12**, 1–9 (2013).
7. Shima, N., Munroe, R. J. & Schimenti, J. C. The mouse genomic instability mutation *chaos1* is an allele of *Polq* that exhibits genetic interaction with *Atm*. *Mol. Cell. Biol.* **24**, 10381–10389 (2004).
8. Yoshimura, M. *et al.* Vertebrate POLQ and POLB cooperate in base excision repair of oxidative DNA damage. *Mol. Cell* **24**, 115–125 (2006).
9. Muzzini, D. M., Plevani, P., Boulton, S. J., Cassata, G. & Marini, F. *Caenorhabditis elegans* POLQ-1 and HEL-308 function in two distinct DNA interstrand cross-link repair pathways. *DNA Repair* **7**, 941–950 (2008).
10. McVey, M. & Lee, S. E. MMEJ repair of double-strand breaks (director's cut): deleted sequences and alternative endings. *Trends in Genet.* **24**, 529–538 (2008).
11. Chan, S. H., Yu, A. M. & McVey, M. Dual roles for DNA polymerase theta in alternative end-joining repair of double-strand breaks in *Drosophila*. *PLoS Genet.* **6**, e1001005 (2010).
12. Yu, A. M. & McVey, M. Synthesis-dependent microhomology-mediated end joining accounts for multiple types of repair junctions. *Nucleic Acids Res.* **38**, 5706–5717 (2010).
13. Koole, W. *et al.* A polymerase theta-dependent repair pathway suppresses extensive genomic instability at endogenous G4 DNA sites. *Nat. Commun.* **5**, 3216 (2014).
14. Nakanishi, K. *et al.* Human Fanconi anemia monoubiquitination pathway promotes homologous DNA repair. *Proc. Natl Acad. Sci. USA* **102**, 1110–1115 (2005).
15. Moldovan, G. L. *et al.* Inhibition of homologous recombination by the PCNA-interacting protein PARI. *Mol. Cell* **45**, 75–86 (2012).
16. Ira, G., Malkova, A., Liberi, G., Foiani, M. & Haber, J. E. Srs2 and Sgs1-Top3 suppress crossovers during double-strand break repair in yeast. *Cell* **115**, 401–411 (2003).
17. Ward, J. D. *et al.* Overlapping mechanisms promote postsynaptic RAD-51 filament disassembly during meiotic double-strand break repair. *Mol. Cell* **37**, 259–272 (2010).
18. Seki, M., Marini, F. & Wood, R. D. POLQ (Pol theta), a DNA polymerase and DNA-dependent ATPase in human cells. *Nucleic Acids Res.* **31**, 6117–6126 (2003).
19. Jackson, D. A. & Pombo, A. Replicon clusters are stable units of chromosome structure: evidence that nuclear organization contributes to the efficient activation and propagation of S phase in human cells. *J. Cell Biol.* **140**, 1285–1295 (1998).
20. The Cancer Genome Atlas Research Network. Integrated genomic characterization of endometrial carcinoma. *Nature* **497**, 67–73 (2013).
21. Morrison, C. *et al.* The controlling role of ATM in homologous recombinational repair of DNA damage. *EMBO J.* **19**, 463–471 (2000).
22. Parmar, K. *et al.* Hematopoietic stem cell defects in mice with deficiency of Fancd2 or Usp1. *Stem Cells* **28**, 1186–1195 (2010).
23. Hu, Y. *et al.* PARP1-driven poly-ADP-ribosylation regulates BRCA1 function in homologous recombination mediated DNA repair. *Cancer Discov.* **4**, 1430–1447 (2014).
24. Yang, D. *et al.* Association of BRCA1 and BRCA2 mutations with survival, chemotherapy sensitivity, and gene mutator phenotype in patients with ovarian cancer. *J. Am. Med. Assoc.* **306**, 1557–1565 (2011).
25. Seki, M. *et al.* High-efficiency bypass of DNA damage by human DNA polymerase Q. *EMBO J.* **23**, 4484–4494 (2004).
26. Seki, M. & Wood, R. D. DNA polymerase theta (POLQ) can extend from mismatches and from bases opposite a (6–4) photoproduct. *DNA Repair* **7**, 119–127 (2008).
27. Zhang, Y. & Jasin, M. An essential role for CtIP in chromosomal translocation formation through an alternative end-joining pathway. *Nature Struct. Mol. Biol.* **18**, 80–84 (2011).
28. Chiruvella, K. K., Liang, Z. & Wilson, T. E. Repair of double-strand breaks by end joining. *Cold Spring Harb. Perspect. Biol.* **5**, a012757 (2013).
29. Alexandrov, L. B. *et al.* Signatures of mutational processes in human cancer. *Nature* **500**, 415–421 (2013).
30. Lemée, F. *et al.* DNA polymerase theta up-regulation is associated with poor survival in breast cancer, perturbs DNA replication, and promotes genetic instability. *Proc. Natl Acad. Sci. USA* **107**, 13390–13395 (2010).

Supplementary Information is available in the online version of the paper.

Acknowledgements We thank N. Shima, D. Chowdhury, G. Shapiro, J. Walter, D. Kozono, J. Ablain, M. Delord, J.-B. Lazaro and members of the D'Andrea laboratory for discussions. We also thank H. Kim for providing DNA constructs, L. Moldovan for providing GST tagged RAD51, S. Johnson for providing MDA-MB 436 cells, A. Y. Li for technical assistance, L. Moreau for chromosomal breakage analysis, and K. Mouw for critical reading of the manuscript. We thank H. Zhang for providing access to shRNA screening data shown in Extended Data Fig. 6i. We thank C. Cazaux and J.-S. Hoffmann for providing pcDNA Flag-tagged Polθ. R.C. received support from the Philippe Foundation and is a recipient of the Ovarian Cancer Research Fellowship (OCRF). This work was supported by NIH grants P50CA168504 and R01HL52725 and by grants from OCRF and BCRF.

Author Contributions R.C. conceived the study, performed experiments, and wrote the manuscript. J.C.L. and T.Y. purified Polθ fragments from insect cells and performed ATPase and gel shift assays. R.A. performed D-loop formation assays. I.H. and S.J.E. performed the DNA fibres assay. B.P. performed mice work and analysed *in vivo* data. M.I.R.P. and S.J.B. performed the Polθ peptide array and the RAD51–ssDNA filament assembly and release assays. K.W.O. scored RAD51 foci. P.A.K. curated TCGA datasets for Figure 3a and Extended Data Figures 5h and 9e and provided clinical perspectives. A.D.D. conceived the study and wrote the manuscript. All authors approved the final version of the manuscript.

Author Information Reprints and permissions information is available at www.nature.com/reprints. The authors declare no competing financial interests. Readers are welcome to comment on the online version of the paper. Correspondence and requests for materials should be addressed to A.D.D. (alan_dandrea@dfci.harvard.edu).

METHODS

Bioinformatic analysis. Gene Set Enrichment Analysis algorithm (GSEA, <http://www.broadinstitute.org>) was performed for the data sets summarized in Supplementary Table 1. TransLesion Synthesis (TLS) and polymerase gene sets are described in Supplementary Table 3. Row expression data were downloaded from Gene Expression Omnibus (GEO). Quantile normalizations were performed using the RMA routine through GenePattern. GSEA was run using GenePattern (<http://www.broadinstitute.org>) and corresponding *P* values were computed using 2,000 permutations. The DNA repair gene set used in Extended Data Fig. 1g has been determined according to a list of 151 DNA genes previously used³¹. GSEA analysis for 151 repair genes has been performed on the ovarian serous data sets (GSE14001, GSE14007, GSE18520, GSE16708, GSE10971). The list of 20 genes shown in Extended Data Fig. 1g represents the top 20 expressed gene in cancer samples (median of the 5 data sets). The waterfall plot in Extended Data Fig. 1h was generated as follows: the 20 genes defined in Extended Data Fig. 1g were used as a gene set; GSEA for indicated data sets was performed and the nominal *P* values were plotted. Supervised analysis of gene expression for GSE9891 was performed with respect to differential expression that differentiated the third of tumours with highest *POLQ* expression from the two-thirds with lowest *POLQ* levels. A list of the 200 most differentially expressed probe sets between the 2 groups (Supplementary Table 2) with false discovery rate <0.05 was analysed for biological pathways (hypergeometrical test; <http://www.broadinstitute.org>). TCGA data sets were accessed through the public TCGA data portal (<https://tcga-data.nci.nih.gov/tcga/>). Fig. 3a reflects *POLQ* gene expression in the ovarian carcinoma data set GSE9891, uterine carcinoma TCGA and breast carcinoma TCGA. Normalization of *POLQ* expression values across data sets was performed using z-score transformation. *POLQ* expression values were subdivided in subgroups reflecting the stage of the disease (for GSE9891: grade 3 ovarian serous carcinoma, *n* = 143 compared to type 1 (grade 1) ovarian cancers, *n* = 20; for uterine serous-like tumours, *n* = 60 compared to the rest of the tumours, *n* = 172; for breast basal-like breast carcinoma, *n* = 80 compared to the rest of the tumours, *n* = 421). Progression-free survival curves were generated by the Kaplan–Meier method and differences between survival curves were assessed for statistical significance with the log-rank test. In the absence of a clinically defined cut-off point for *POLQ* expression levels, we divided patients into 2 groups: those with *POLQ* mRNA levels equal to or above the median (*POLQ* high group) and those with values below the median (*POLQ* low group). We then analysed the correlation of *POLQ* with outcome in each group. Patients with cyclin E1 (CCNE1) amplification (resistant to CDDP) were excluded from the analysis. For mutation count, we accessed data from tumours included in the TCGA data sets for which gene expression and whole-exome DNA sequencing was available. Data were accessed through the public TCGA data portal and the cBioPortal for Cancer Genomics (<http://www.cbiportal.org>). For each TCGA data set, non-synonymous mutation count was assessed in tumours with the highest *POLQ* expression (top 33%) and compared to tumours with low *POLQ* expression (the remaining 67%). In the uterine TCGA²⁰, we curated all tumours except the ultra and hyper-mutated group (that is, POLE and MSI tumours). In the breast TCGA³², all tumours were analysed. In the ovarian TCGA¹, we curated tumours harbouring molecular alterations (via mutation and epigenetic silencing) of the HR pathway.

Plasmid construction. To facilitate subcloning, a silent mutation (A390A) was introduced into the *POLQ* gene sequence to remove the unique XbaI cutting site. Full-length or truncated *POLQ* cDNA were PCR-amplified and subcloned into pcDNA3-N-Flag, pFastBac-C-Flag, pOZ-C-Flag-HA, or GFP-C1 vectors to generate the various constructs. Point mutations and loop deletions were introduced by QuikChange II XL Site-Directed Mutagenesis Kit (Agilent Technologies) and confirmed by DNA sequencing. For Pol0 rescue experiments (Fig. 4g, h and Extended Data Fig. 3d, e), *POLQ* cDNA constructs resistant to siPol01 were generated into the pOZ-C-Flag-HA vector and the constructs were stably expressed in indicated cell line by retroviral transduction. The Pol0 ATPase catalytically-dead mutant (A-dead) was generated by mutating the Walker A and B motifs (Walker A: K121A and Walker B: D216A, E217A). pOZ-C-Flag-HA Pol0 constructs were generated for retroviral transduction, and stable cells were selected using magnetic Dynabeads (Life Technologies) conjugated to the IL2R antibody (Millipore).

SiRNA and shRNA sequence information. For siRNA-mediated knockdown, the following target sequences were used: *POLQ* (Qiagen POLQ_1 used as siPol01 and Qiagen POLQ_6 used as siPol02); *BRCA1* (Qiagen BRCA1_13); *PARP1* (Qiagen PARP1_6); *REV1* (5'-CAGCCGAUCUGUGCCAA-TT-3'); *BRCA2* (5'-G AAGAAUGCAGGUUAAAATT-3'); *BLM* (5'-AUCAGCUAGGGCGAUCA ATT-3'); *FANCD2* (5'-GGAGAUUGAUGGCUACUATT-3') and *PAR1* (5'-A GGACACAUAGUAAGGGAUUGCUATT-3'). AllStars negative control siRNA (Qiagen) served as the negative control. ShRNAs targeting human *FANCD2* was previously generated in the pTRIP/DU3-MND-GFP vector³³. ShRNAs targeting human *POLQ* (CGGGCCTTTAGATATAAAT), human *BRCA2* (AAGAAGA ATGCAGGTTAATA) or control (Scr, scramble) were generated in the pLKO-1

vector. *POLQ* (V2THS_198349) and non-silencing TRIPZ-RFP doxycycline-inducible shRNA were purchased from Open Biosystems. All shRNAs were transduced using lentivirus.

Immunoblot analysis, fractionation and pull-down assays. Cells were lysed with 1% NP-40 lysis buffer (1% NP-40, 300 mM NaCl, 0.1 mM EDTA, 50 mM Tris (pH 7.5)) supplemented with protease inhibitor cocktail (Roche), resolved by NuPAGE (Invitrogen) gels, and transferred onto nitrocellulose membrane, followed by detection using the LAS-4000 Imaging system (GE Healthcare Life Sciences). For immunoprecipitation, cells were lysed with 300 mM NaCl lysis buffer, and the lysates were diluted to 150 mM NaCl before immunoprecipitation. Lysates were incubated with anti-Flag agarose resin (Sigma) followed by washes with 150 mM NaCl buffer. *In vitro* transcription and translation reactions were carried out using the TNT T7 Quick Coupled Transcription–Translation System (Promega). For cellular fractionation, cells were incubated with low-salt permeabilization buffer (10 mM Tris (pH 7.3), 10 mM KCl, 1.5 mM MgCl₂) with protease inhibitor on ice for 20 min. Following centrifugation, nuclei were resuspended in 0.2 M HCl and the soluble fraction was neutralized with 1 M Tris-HCl (pH 8.0). Nuclei were lysed in 150 mM NaCl and following centrifugation, the chromatin pellet was digested by micrococcal nuclease (Roche) for 5 min at room temperature. Recombinant GST–RAD51 and GST–PCNA fusion protein were expressed in BL21 strain and purified using glutathione-Sepharose beads (GE Healthcare) as previously described¹⁵. Beads with equal amount of GST or GST–RAD51 were incubated with *in vitro* translated Flag-tagged Pol0 variants in 150 mM NaCl lysis buffer.

Antibodies and chemicals. Antibodies used in this study included: anti-PCNA (PC-10), anti-FANCD2 (FI-17), anti-RAD51 (H-92), anti-GST (B14), and histone H3 (FL-136) and anti-vinculin (H-10) (Santa Cruz); anti-Flag (M2) (Sigma); anti-pS317CHK1 (2344), anti-pT68CHK2 (2661) (Cell signalling); anti-pS824KAP-1 (A300-767A) (Bethyl); anti-pS317γH2AX (05636) (Millipore); anti-pS15p53 (ab1431) and anti-Pol0 (ab80906) (abcam); anti-BrdU (555627) (BD Pharmingen). Mitomycin C (MMC), cis-diamminedichloroplatinum(II) (cisplatin, CDDP), and hydroxyurea (HU) were purchased from Sigma. The PARPi rucaparib (AG-014699) was purchased from Selleckchem and ABT-888 from AbbVie. Rucaparib was used for all *in vitro* assays and ABT-888 was used for all *in vivo* experiments.

Chromosomal breakage analysis. 293T and VU 423 cells were twice-transfected with siRNAs for 48 h and incubated for 48 h with or without the indicated concentrations of MMC. For complementation studies on 293T shFANCD2, *POLQ* cDNA constructs were transfected 24 h after the first siRNA transfection. Cells were exposed for 2 h to 100 ng ml⁻¹ of colcemid and treated with a hypotonic solution (0.075 M KCl) for 20 min and fixed with 3:1 methanol/acetic acid. Slides were stained with Wright's stain and 50 metaphase spreads were scored for aberrations. The relative number of chromosomal breaks was calculated relative to control cells (si Scr). Radial figures were excluded from the analysis for clarity in Fig. 4b.

Reporter assays and immunofluorescence. HR and alt-EJ efficiency was measured using the DR-GFP (HR efficiency) and the alt-EJ reporter assay, performed as previously described^{14,27,34}. Briefly, 48 h before transfection of Scel cDNA, U2OS-DR-GFP cells were transfected with the indicated siRNA or PARPi (1 μM). The HR activity was determined by FACS quantification of viable GFP-positive cells 96 h after Scel was transfected. For RAD51 immunofluorescence experiments, cells were transfected with indicated siRNA 48 h before treatment with HU (2 mM) or IR (10 Gy). For complementation studies, Pol0 cDNA constructs were either transfected 24 h after siRNA transfection (Fig. 2b, c and Extended Data Fig. 9b) or stably expressed in the indicated cell line (Extended Data Fig. 3d, e). 6 h after HU or IR treatment, cells were fixed with 4% paraformaldehyde for 10 min at room temperature, followed by extraction with 0.3% Triton X-100 for 10 min on ice. Antibody staining was performed at room temperature for 1 h. For quantification of RAD51 foci in BrdU positive cells, cells were transfected with indicated siRNA 48 h before treatment with IR (10 Gy). Then 2 h after IR treatment, cells were treated with BrdU pulse (10 μM) for 2 h and subsequently fixed with 4% paraformaldehyde and stained for RAD51 as described above. Cells were then fixed in ethanol (4 °C, overnight), treated with 1.5 M HCl for 30 min and stained for BrdU antibody. The relative number of cells with more than 10 RAD51 foci was calculated relative to control cells (si Scr). Statistical differences between cells transfected with siRNAs (si Pol01, si Pol02, si BRCA2, si PARI or si BLM relative to control (si Scr) were assessed. For GFP fluorescence, cells were grown on coverslips, treated with UV (24 h after GFP–Pol0 transfection; 20 J m⁻²), fixed with 4% paraformaldehyde for 10 min at 25 °C 4 h after the UV treatment, washed three times with PBS and mounted with DAPI-containing mounting medium (Vector Laboratories). When indicated, cells were treated with PARPi (1 μM) 24 h before GFP–Pol0 transfection. Images were captured using a Zeiss AXIO10 fluorescence microscope and AxioVision software. Cells with GFP foci were quantified by counting number of cells with more than five foci. At least 150 cells were counted for each sample.

Cell survival assays. For assessing cellular cytotoxicity, cells were seeded into 96-well plates at a density of 1,000 cells per well. Cytotoxic drugs were serially diluted

in media and added to the wells. At 72 h, CellTiter-Glo reagent (Promega) was added to the wells and the plates were scanned using a luminescence microplate reader. Survival at each drug concentration was plotted as a percentage of the survival in drug-free media. Each data point on the graph represents the average of three measurements, and the error bars represent the standard deviation. For clonogenic survival, 1,000 cells per well were seeded into 6-well plates and treated with cytotoxic drugs the next day. For MMC and PARPi, cells were treated continuously with indicated drug concentrations. For CDDP, cells were treated for 24 h and cultured for 14 days in drug-free media. Colony formation was scored 14 days after treatment using 0.5% (w/v) crystal violet in methanol. Survival curves were expressed as a percentage \pm s.e.m. over three independent experiments of colonies formed relative to the DMSO-treated control.

Cell cycle analysis. A2780 cells expressing Scr or Pol θ shRNA were synchronized by a double thymidine block (Sigma) and subsequently exposed to MMC (1 $\mu\text{g ml}^{-1}$ for 2 h), IR (10 Gy) or HU (2 mM, overnight). At the indicated time points following drug release, cells were fixed in chilled 70% ethanol, stored overnight at -20°C , washed with PBS, and resuspended in propidium iodide. A fraction of those cells was analysed by immunoblotting for DNA damage response proteins. The immunoblot analysis of γ H2AX shows staining after 0, 24, 48 and 72 h of HU treatment. For proliferation experiments, cells were incubated with 5-ethynyl-2'-deoxyuridine (EdU) (10 μM) for 1 h at each time point after MMC exposure (1 $\mu\text{g ml}^{-1}$ for 2 h). Cells were washed and resuspended in culture medium for 2 h before being analysed by flow cytometry. EdU staining was performed using the Click-iT EdU kit (Life Technologies).

DNA fibre analysis. A2780 cells expressing Scr or Pol θ shRNA were incubated with 25 μM chlorodeoxyuridine (Cl d U) (Sigma, C6891) for 20 min. Cells were then treated with 2 mM hydroxyurea (HU) for 2 h and incubated in 250 μM iododeoxyuridine (Id d U) (Sigma, I7125) for 25 min after washout of the drug. Spreading of DNA fibres on glass slides was done as previously reported¹⁹. Glass slides were then washed in distilled water and in 2.5 M HCl for 80 min followed by three washes in PBS. The slides were incubated for 1 h in blocking buffer (PBS with 1% BSA and 0.1% NP-40) and then for 2 h in rat anti-BrdU antibody (1:250, Abcam, ab6326). After washing with blocking buffer, the slides were incubated for 2 h in goat anti-rat Alexa 488 antibody (1:1,000, Life Technologies, A-11006). The slides were then washed with PBS and 0.1% NP-40 and then incubated for 2 h with mouse anti-BrdU antibody diluted in blocking buffer (1:100, BD Biosciences, 347580). Following an additional wash with PBS and 0.1% NP-40, the fibres were stained for 2 h with chicken anti-mouse Alexa 594 (1:1000, Life Technologies, A-21201). At least 150 fibres were counted per condition. Pictures were taken with an Olympus confocal microscope and the fibres were analysed by ImageJ software. The number of stalled or collapsed forks were measured by DNA fibres that had incorporated only Cl d U. Stalled or collapsed forks counted in Pol θ -depleted cells is expressed as fold-change after HU treatment relative to the fold-change observed in control cells, which was arbitrarily set to 1.

SupF mutagenesis assay. 293T cells twice-transfected with siRNAs for 48 h were then transfected with undamaged or damaged (UVC, 1,000 J m $^{-2}$) pSP189 plasmids using GeneJuice (Novagen). After 48 h, plasmid DNA was isolated with a miniprep kit (Promega) and digested with DpnI. After ethanol precipitation, extracted plasmids were transformed into the β -galactosidase-MBM7070 indicator strain through electroporation (GenePulsor X Cell; Bio-Rad) and plated onto LB plates containing 1 mM IPTG, 100 $\mu\text{g ml}^{-1}$ 5-bromo-4-chloro-3-indolyl- β -D-galactopyranoside and 100 $\mu\text{g ml}^{-1}$ ampicillin. White and blue colonies were scored using ImageJ software, and the mutation frequency was calculated as the ratio of white (mutant) to total (white plus blue) colonies.

POLQ gene expression. RNA samples extracted using the TRIzol reagent (Invitrogen) were reverse transcribed using the Transcripter Reverse Transcriptase kit (Roche) and oligo dT primers. The resulting cDNA was used to analyse POLQ expression by RT-qPCR using with QuantiTect SYBRGreen (Qiagen), in an iCycler machine (Bio-Rad). POLQ gene expression values were normalized to expression of the housekeeping gene GAPDH, using the ΔCt method and are shown on a log₂ scale. The primers used for POLQ are as follows: POLQ primer 1 (forward: 5'-TATCTGCTGGAACTTTGCTGA-3'; reverse: 5'-CTCACACCATTCTTGATGGA-3'); POLQ primer 2 (forward: 5'-CTACAAGTGAAGGGAGATGAGG-3'; reverse: 5'-TCAGAGGGTTTACCAATCC-3').

Pol θ purification from insect SF9 cells. A Pol θ fragment (ΔPol2) containing the ATPase domain with a RAD51 binding site (amino acids 1 to 1,000) was cloned into pFastBac-C-Flag and purified from baculovirus-infected SF9 insect cells as previously described³⁵. Briefly, SF9 cells were seeded in 15-cm dishes at 80–90% confluence and infected with baculovirus. Three days post-infection, cells were collected and lysed in 500 mM NaCl lysis buffer (500 mM NaCl, 0.01% NP-40, 0.2 mM EDTA, 20% glycerol, 1 mM DTT, 0.2 mM PMSF, 20 mM Tris (pH 7.6)) supplemented with Halt protease inhibitor cocktail (Thermo Scientific) and calpain I inhibitor (Roche) and the protein was eluted in lysis buffer supplemented with

0.2 mg ml $^{-1}$ of Flag peptide (Sigma). The protein was concentrated in lysis buffer using 10 kDa centrifugal filters (Amicon). The protein was quantified by comparing its staining intensity (Coomassie-R250) with that of BSA standards in a 7% Tris-glycine SDS-PAGE gel. Purified protein was flash-frozen in small aliquots in liquid nitrogen and stored at -80°C .

Radiometric ATPase assay. Each 10 μl reaction consisted of 200 nM ATP, reaction buffer (20 mM Tris-HCl (pH 7.6), 5 mM MgCl $_2$, 0.05 mg ml $^{-1}$ BSA, 1 mM DTT), and 5 μCi of [γ -³²P]ATP. For corresponding reactions, ssDNA, dsDNA, and forked DNA were added to the reaction in excess at a final concentration of 600 nM. Once all of the non-enzymatic reagents were combined, recombinant Pol θ was added to start the ATPase reaction. After incubation for 90 min at room temperature, stop buffer (125 mM EDTA (pH 8.0)) was added and approximately \sim 0.05 μCi was spotted onto PEI-coated thin-layer chromatography (TLC) plates (Sigma). Unhydrolyzed [γ -³²P]ATP was separated from the released inorganic phosphate [³²P] $_i$ with 1 M acetic acid, 0.25 M lithium chloride as the mobile phase. TLC plates were exposed to a phosphor screen and imaged with the BioRad Imager PMC. ssDNA, dsDNA, and forked DNA were generated as previously described³⁵. To remove any contaminating ssDNA, dsDNA and forked DNA were gel purified after annealing. Spots corresponding to [γ -³²P]ATP and the released inorganic phosphate [³²P] $_i$ were quantified (in units of pixel intensity) and the fraction of ATP hydrolysed calculated for each Pol θ concentration.

Electrophoretic mobility gel shift assay (EMSA). Binding of Pol θ to ssDNA was assessed using EMSA. 60-mer single-stranded DNA (ssDNA) or double-stranded DNA (dsDNA) oligonucleotides (5 nM) were incubated with increasing amount of Pol θ (0, 5, 10, 50, or 100 nM) in 10 μl of binding buffer (20 mM HEPES-K $^+$, (pH 7.6), 5 mM magnesium acetate, 0.1 $\mu\text{g ml}^{-1}$ BSA, 5% glycerol, 1 mM DTT, 0.2 mM EDTA, and 0.01% NP-40) for 1 h on ice. Pol θ protein was added at a tenfold dilution so that the final salt concentration was approximately 50 mM NaCl. The ssDNA probes were 5' fluorescently labelled with IRDye-700 (IDT). After incubation, the samples were analysed on a 5% native polyacrylamide/0.5X TBE gel at 4 °C. A fluorescent imager (Li-Cor) was used to visualize the samples in the gel.

RAD51 purification. Human GST-RAD51 was purified from bacteria as described³⁶. *Xenopus* Rad51 (xRad51) was purified as follows. N-terminally His-tagged SUMO-Rad51 was expressed in BL21 pLysS cells. Three hours after induction with 1 mM IPTG, cells were collected and resuspended in buffer A (50 mM Tris-Cl (pH 7.5), 350 mM NaCl, 25% sucrose, 5 mM β -mercaptoethanol, 1 mM PMSF and 10 mM imidazole). Cells were lysed by supplementation with Triton X-100 (0.2% final concentration), three freeze-thaw cycles and sonication (20 pulses at 40% efficiency). The soluble fraction was separated by centrifugation and incubated with 2 ml of Ni-NTA resin (Qiagen) for 1 h at 4 °C. After washing the resin with 100 ml of wash buffer (buffer A supplemented with 1 M NaCl, final concentration), the salt concentration was brought down to 350 mM. His-SUMO-Rad51 was eluted with a linear gradient of imidazole from 10–300 mM in buffer A. Eluted fractions were analysed by SDS-PAGE. His-SUMO-Rad51 containing fractions were pooled and supplemented with Ulp1 protease to cleave the His-SUMO tag and dialysed overnight into buffer B (50 mM Tris-Cl (pH 7.5), 350 mM NaCl, 25% sucrose, 10% glycerol, 5 mM β -mercaptoethanol, 10 mM imidazole and 0.05% Triton X-100). The dialysed fraction was incubated with Ni-NTA resin for 1 h at 4 °C and the Rad51 containing flow-through fraction was collected and dialysed overnight into buffer C (100 mM potassium phosphate (pH 6.8), 150 mM NaCl, 10% glycerol, 0.5 mM DTT and 0.01% Triton-X). Rad51 was further purified by hydroxyapatite (Bio-Rad) chromatography. After washing with ten column volumes of buffer C, Rad51 was eluted with a linear gradient of potassium phosphate (pH 6.8) from 100–800 mM. Rad51 containing fractions were analysed by SDS-PAGE and dialysed into storage buffer (20 mM HEPES-KOH (pH 7.4), 150 mM NaCl, 10% glycerol, 0.5 mM DTT). Purified protein was flash-frozen in small aliquots in liquid nitrogen and stored at -80°C .

D-loop assay. D-loop formation assays were performed using xRad51 and conducted as previously described³⁷. Briefly, nucleofilaments were first formed by incubating RAD51 (1 μM) with end-labelled 90-mer ssDNA (3 μM nt) at 37 °C for 10 min in reaction buffer containing 20 mM HEPES-KOH (pH 7.4), 1 mM ATP, 1 mM MgCl $_2$, 1 mM DTT, BSA (100 $\mu\text{g ml}^{-1}$), 20 mM phosphocreatine and creatine phosphokinase (20 $\mu\text{g ml}^{-1}$). After the 10 min incubation, increasing amounts of Pol θ (0, 0.1, 0.5, or 1.0 μM) and RPA (200 nM) were added and incubated for an additional 15 min at 37 °C. The reaction was then supplemented with 1 mM CaCl $_2$ followed by further incubation at 37 °C for 15 min. D-loop formation was initiated by the addition of supercoiled dsDNA (pBS-KS (-), 79 μM bp) and incubation at 37 °C for 15 min. D-loops were analysed by electrophoresis on a 0.9% agarose gel after deproteinization. Gel was dried and exposed to a PhosphoImager (GE Healthcare) screen for quantification.

Substitution peptide arrays and RAD51-ssDNA filament experiments. Substitution peptide arrays were performed as previously described¹⁷. RAD51 displacement assays were performed as follows. Binding reactions (10 μl) contained 5' -³²P-end-labelled

DNA substrates (0.5 ng of 60 mer ssDNA) and various amounts of human RAD51 and/or Pol θ in binding buffer (40 mM Tris-HCl (pH 7.5), 50 mM NaCl, 10 mM KCl, 2 mM DTT, 5 mM ATP, 5 mM MgCl₂, 1 mM DTT, 100 mg ml⁻¹ BSA) were conducted at room temperature. After 5 min incubation with Pol θ and a further 5 min incubation with RAD51 or vice versa, an equimolar amount of cold DNA substrate was added to the reaction. Products were then analysed by electrophoresis through 10% PAGE (200 V for 40 min in 0.5× Tris-borate-EDTA buffer) and visualized by autoradiography.

Interbreeding of the *Fancd2* and *Polq* mice. For the characterization of *Fancd2*/*Polq* conditional knockouts, we crossed C57BL/6J mice (Jackson Laboratory). *Fancd2*^{+/−}/*Polq*^{+/−} mice, previously generated in our laboratory²², were crossed with *Fancd2*^{+/−}/*Polq*^{+/−} mice² to generate *Fancd2*^{+/−}/*Polq*^{+/−} mice. These double heterozygous mice were then interbred, and the offspring from these mating pairs were genotyped using PCR primers for *Fancd2* and *Polq*. A statistical comparison of the observed with the predicted genotypes was performed using a two-sided Fisher's exact test. Primary MEFs were generated from E13.5 to E15 embryos and cultured in RPMI supplemented with 15% fetal bovine serum and 1% penicillin-streptomycin. All data generated in the study were extracted from experiments performed on primary MEFs from passage 1 to passage 4. The primers used for mice genotyping are as follows: *Fancd2* PCR primers OST2cF (5'-CATGCATATAGGAACCGAAGG-3'), OST2aR (5'-CAGGACCTTGGAGAACAG-3') and LTR2bF (5'-GCGTTACTTAAGCTAGCTTG-3'); *Polq* PCR primers IMR5973 (5'-TGCAGTG TACAGATGTTACTTT-3'), IMR5974 (5'-TGGAGGTAGCATTCTCTC-3'), IMR5975 (5'-TCACTAGGTTGGGGTCTC-3') and IMR5976 (5'-CATCAGAAGCTGACTCTAGAG-3'). Specific PCR conditions are available upon request.

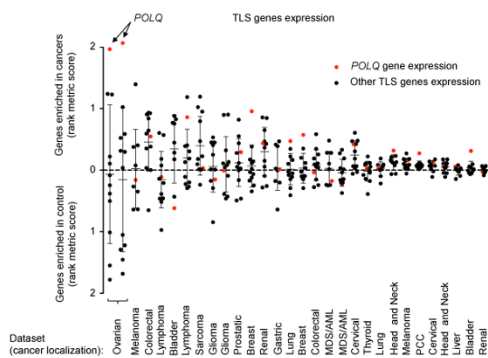
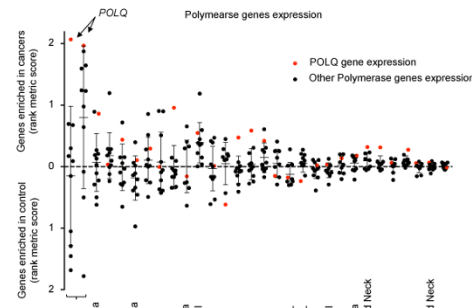
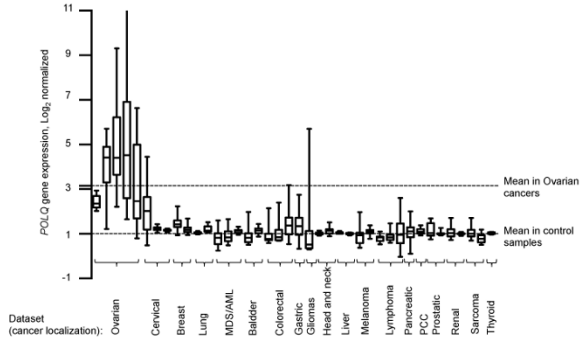
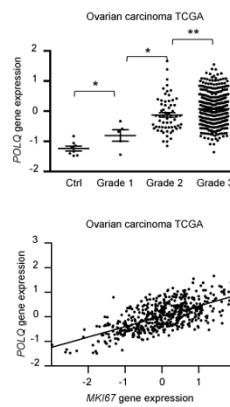
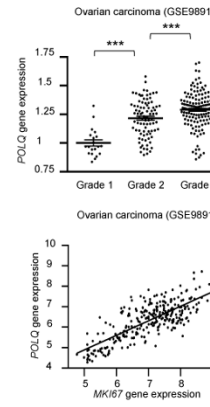
Studies of xenograft-bearing CrTac:NCr-Foxn1nu mice. The Animal Resource Facility at The Dana-Farber Cancer Institute approved all housing situations, treatments and experiments using mice. No more than five mice were housed per air-filtered cage with *ad libitum* access to standard diet and water, and were maintained in a temperature- and light-controlled animal facility under pathogen-free conditions. All mice described in this text were drug and procedure naive before the start of the experiments. For every xenograft study, we subcutaneously implanted approximately 1.0×10^6 A2780 cells (1:1 in Matrigel Matrix, BD Biosciences) into both flanks of 6–8-week-old female CrTac:NCr-Foxn1nu mice (Taconic). Doxycycline (Sigma) was added to the food (625 p.p.m.) and bi-weekly (Tuesday and Friday) to the water (200 µg ml⁻¹) for mice bearing tumours that reached 100–200 mm³. Roughly one week (5–6 days) after the addition of doxycycline to the diet, mice were randomized to twice daily treatment schedules with vehicle (0.9% NaCl) or PARPi (ABT-888; 50 mg per kg body weight) by oral gavage administration for the indicated number of weeks. Overall survival was determined using Kaplan-Meier analyses performed with log-rank tests to assess differences in median survival for each shRNA condition (shScr or shPol θ) and each treatment condition (vehicle or PARPi) (GraphPad Prism 6 Software). For competition assays, A2780 cells expressing FANCD2-GFP shRNA (GFP positive cells) or a combination of FANCD2-GFP shRNA with (doxycycline inducible) Scr-RFP or Pol θ -RFP shRNA (GFP-RFP positive cells) were mixed at an equal ratio of GFP to GFP-RFP positive cells, and thereafter injected into nude mice given doxycycline-containing diets and treated with either vehicle or PARPi or CDDP. For competition assays, mice received identical doxycycline and PARPi drug treatment. For the cisplatin

competition assay, mice were randomized into semi-weekly treatment regimens with vehicle (0.9% NaCl) or CDDP (5 mg per kg body weight) by intraperitoneal injection. After three to four weeks of treatment, mice were euthanized and tumours were grown *in vitro*, in the presence of doxycycline (2 µg ml⁻¹ for 4 days). The relative ratio of GFP to GFP-RFP positive cells was determined by FACS analysis. Tumour volumes were calculated bi-weekly using caliper measurements (length × width²)/2. Growth curves were plotted as the mean tumour volume (mm³) for each treatment group; relative tumour volume (RTV) indicates the change in tumour volume at a given time point relative to the tumour volume at the day of initial measurement (volume of approximately 0.15 cm³) which was arbitrarily set to 1. Mice were unbiasedly assigned into different treatment groups. Drug treatment and outcome assessment was performed in a blinded manner. Mice were monitored every day and euthanized by CO₂ inhalation when tumour size (≥ 2 cm), tumour status (necrosis/ulceration) or body weight loss ($\geq 20\%$) reached ethical endpoint, according to the rules of the Animal Resource Facility at The Dana-Farber Cancer Institute.

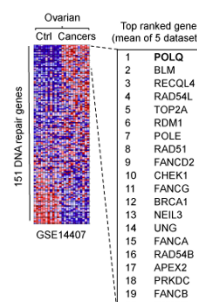
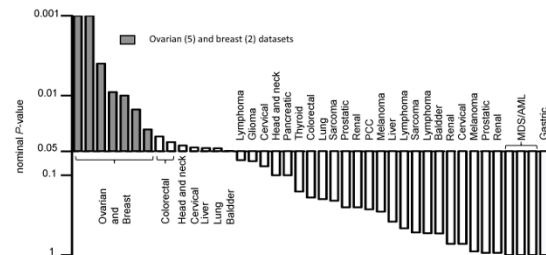
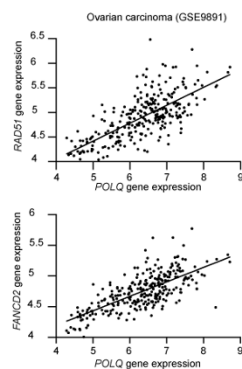
Immunohistochemical staining. We stained formalin-fixed paraffin-embedded sections of harvested xenografts with antibodies specific for γH2AX (pSer139) (Upstate Biotechnology) and Ki67 (Dako). At least two xenografts were scored for each treatment. Tumours were collected 3 weeks after treatment. At least five 40 × fields were scored. The mean ± s.e.m. percentage of positive cells from five images in each treatment group was calculated.

Statistical analysis. Unless stated otherwise, all data are represented as mean ± s.e.m. over at least three independent experiments, and significance was calculated using the Student's *t*-test. Asterisks indicate statistically significant (**P* < 0.05; ***P* < 10⁻²; ****P* < 10⁻³) values. All the *in vivo* experiments were run with at least 6 tumours from 6 mice for each condition. No statistical methods were used to predetermine sample size.

31. Kang, J., D'Andrea, A. D. & Kozono, D. A DNA repair pathway-focused score for prediction of outcomes in ovarian cancer treated with platinum-based chemotherapy. *J. Natl. Cancer Inst.* **104**, 670–681 (2012).
32. The Cancer Genome Atlas Network Comprehensive molecular portraits of human breast tumours. *Nature* **490**, 61–70 (2012).
33. Ceccaldi, R. et al. Bone marrow failure in Fanconi anemia is triggered by an exacerbated p53/p21 DNA damage response that impairs hematopoietic stem and progenitor cells. *Cell Stem Cell* **11**, 36–49 (2012).
34. Bennardo, N., Cheng, A., Huang, N. & Stark, J. M. Alternative-NHEJ is a mechanistically distinct pathway of mammalian chromosome break repair. *PLoS Genet.* **4**, e1000110 (2008).
35. Yusufzai, T. & Kadonaga, J. T. HARP is an ATP-driven annealing helicase. *Science* **322**, 748–750 (2008).
36. Barber, L. J. et al. RTEL1 maintains genomic stability by suppressing homologous recombination. *Cell* **135**, 261–271 (2008).
37. Amunugama, R., Groden, J. & Fishel, R. The HsRAD51B-HsRAD51C stabilizes the HsRAD51 nucleoprotein filament. *DNA Repair* **12**, 723–732 (2013).
38. Pitroda, S. P. et al. DNA repair pathway gene expression score correlates with repair proficiency and tumor sensitivity to chemotherapy. *Sci. Transl. Med.* **6**, 229ra242 (2014).
39. Aggarwal, M., Sommers, J. A., Shoemaker, R. H. & Brosh, R. M., Jr. Inhibition of helicase activity by a small molecule impairs Werner syndrome helicase (WRN) function in the cellular response to DNA damage or replication stress. *Proc. Natl. Acad. Sci. USA* **108**, 1525–1530 (2011).

a**b****c****d****e****f**

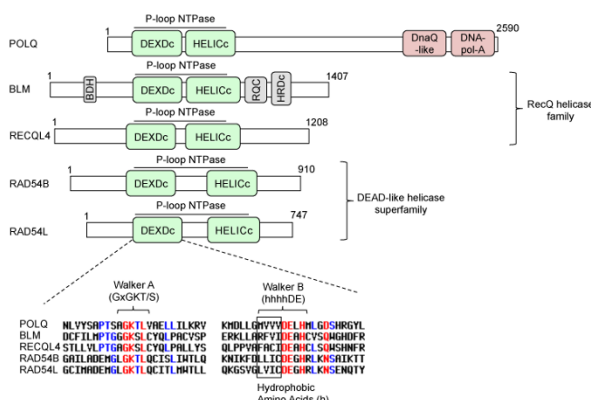
Gene Ontology (GO) Biological process	Number of GO term	P value (mean)
Cell cycle	8	1.51042E-05
Mitosis and cytokinesis	46	5.44857E-05
Homologous recombination	4	5.27823E-05
Checkpoint	3	6.00749E-07

**h****i****j**

POLQ	DNA repair activity
TOPBP1	yes
BLM	yes
RAD54L	yes
PLK4	no
FANCI	yes
SMC4	no
BRCA1	yes
FANCD2	yes
ATAD5	yes
TRAIP	no

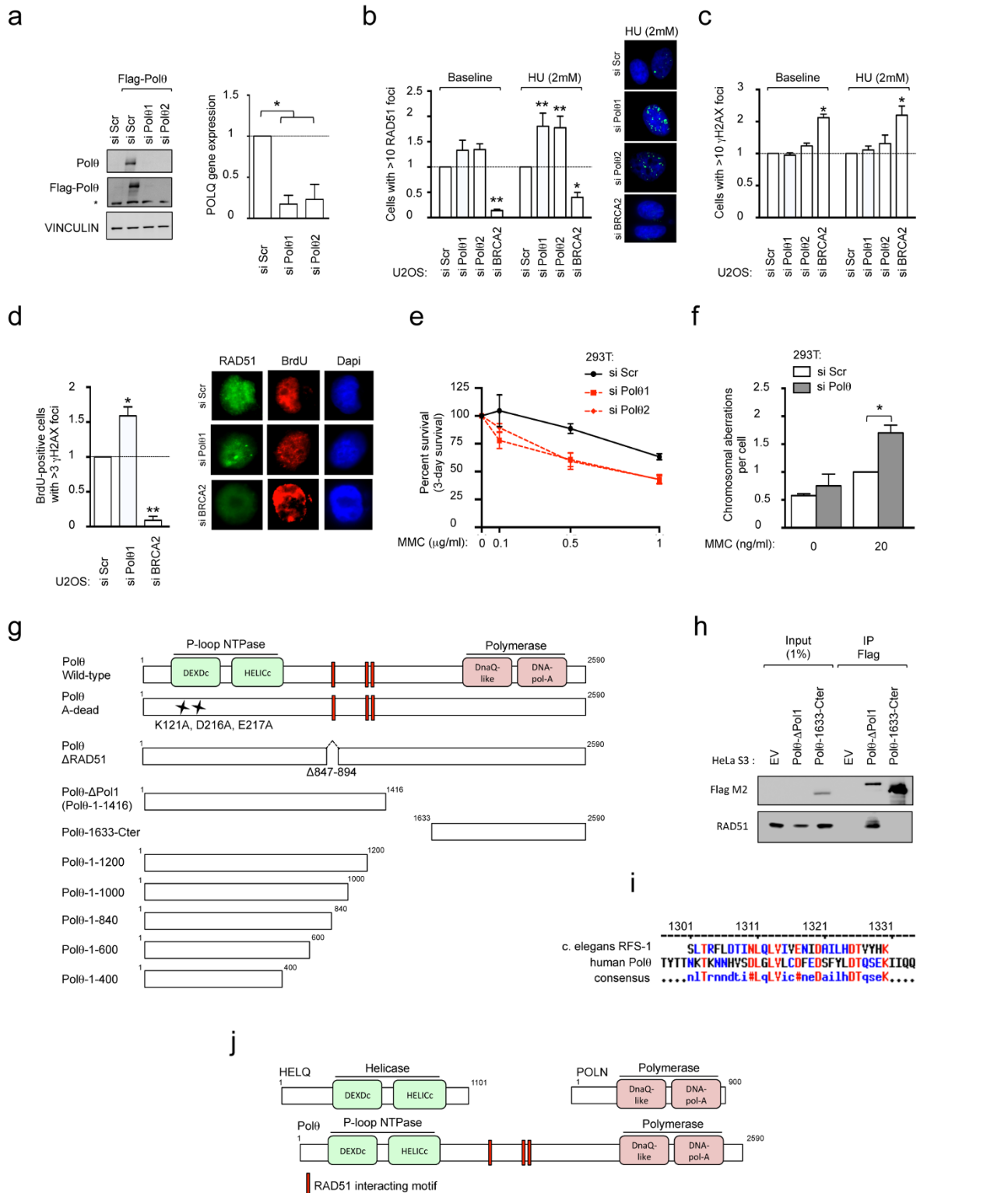
k

Gene Ontology (GO) molecular function	GO ID	P value
DNA helicase activity	GO:0003678	0.00002
helicase activity	GO:0004386	0.0001
nucleoside-triphosphatase activity	GO:0017111	0.0002
pyrophosphatase activity	GO:0016462	0.0002
hydrolase activity, acting on acid anhydrides	GO:0016817	0.0002
hydrolase activity, acting on acid anhydrides, in phosphorus-containing anhydrides	GO:0016818	0.0002
catalytic activity	GO:0003824	0.0003
DNA-directed DNA polymerase activity	GO:0003887	0.0003
DNA polymerase activity	GO:0034061	0.0005
damaged DNA binding	GO:0003684	0.0009



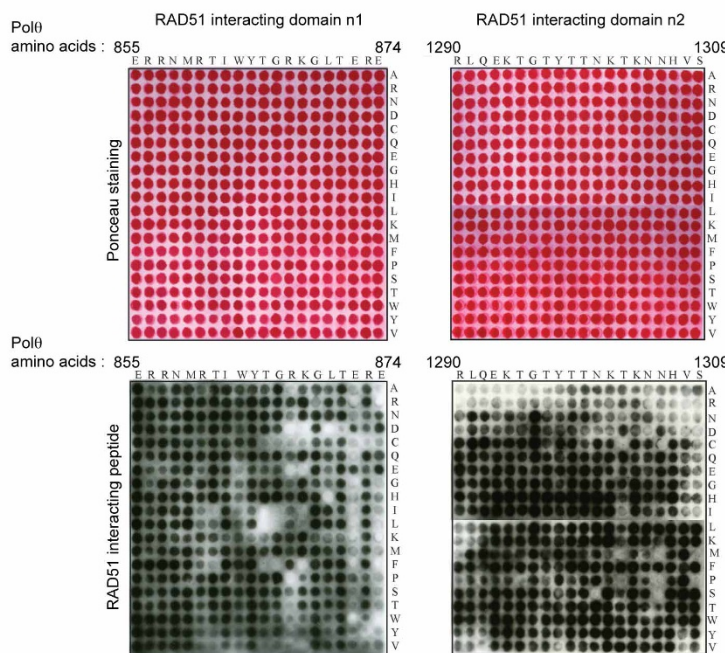
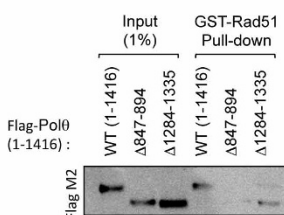
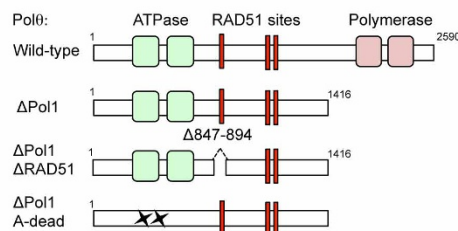
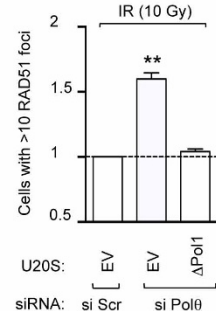
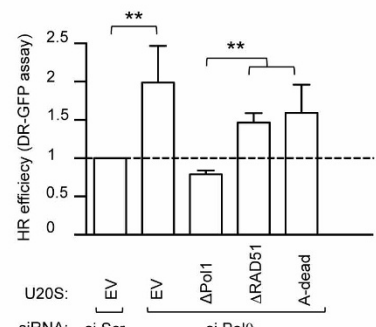
Extended Data Figure 1 | *POLQ* is highly expressed in epithelial ovarian cancers (EOCs) and *POLQ* expression correlates with expression of HR genes. **a, b,** Gene set enrichment analysis (GSEA) for expression of TransLesion Synthesis (TLS) (**a**) and polymerase (**b**) genes between primary cancers and control samples in 28 independent data sets from 19 different cancer types. Enrichment values (represented as a single dot for each gene in a defined data set) were determined using the rank metric score to compare expression values between cancers and control samples. Dots above the dashed line reflect enrichment in cancer samples, whereas dots below the dashed line show gene expression enriched in control samples. Data sets were ranked based on the amplitude of the rank metric score and plotted as shown. **c,** *POLQ* gene expression in 40 independent data sets from 19 different cancer types. For each data set, *POLQ* values were expressed as fold-change differences relative to the mean expression in control samples, which was arbitrarily set to 1. **d,** *POLQ* expression correlates with tumour grade and MKi67 gene expression in the ovarian TCGA ($n = 494$ patients with ovarian carcinoma (grade 1, $n = 5$; grade 2, $n = 61$; grade 3, $n = 428$) and control samples, $n = 8$). **e,** *POLQ* expression correlates with tumour grade MKi67 gene expression in the ovarian data set GSE9891 ($n = 251$ patients with ovarian serous and endometrioid carcinoma for which grade status was available (grade 1, $n = 20$; grade 2, $n = 88$; grade 3, $n = 143$)). Statistical correlation was assessed using the Pearson test (for **d**: $r = 0.65$, $P < 10^{-3}$; for **e**: $r = 0.77$, $P < 10^{-3}$). **f,** Top-ranked biological pathways differentially expressed between samples expressing high levels of *POLQ* (high *POLQ*, first 33%, $n = 95$) relative to samples with low *POLQ* expression (low *POLQ*, 67%, $n = 190$) on the ovarian data set GSE9891 ($n = 285$ patients with ovarian carcinoma). Significance values were determined by the hypergeometrical test using the 200 most differentially expressed probe sets between the 2 groups (high *POLQ* and low *POLQ*). **g,** GSEA for expression of DNA repair genes between primary cancers

and control samples in 5 independent ovarian cancer data sets. A representative heat map showing differential gene expression between ovarian cancers and controls is shown from GSE14407. For each data set, DNA repair genes were ranked based on the metric score reflecting their enrichment in cancer samples. The top 20 DNA repair genes primarily expressed in cancer samples compared to control samples is shown on the right. **h,** GSEA for the top 20 DNA repair genes defined in **g** between primary cancers and control samples in 40 independent cancer data sets. The nominal P value was used as a measure of the expression enrichment in cancer samples and represented as a waterfall plot. When the gene set expression was enriched in control samples, the P value was arbitrarily set to 1. **i,** *POLQ* expression correlates with *RAD51* and *FANCD2* gene expression in 285 samples from the ovarian data set GSE9891. Statistical correlation was assessed using the Pearson test ($r = 0.71$, $P < 10^{-3}$). **j,** Top 10 genes that most closely correlated with *POLQ* expression (gene neighbours analysis) for 1,046 cell lines from the CCLE collection. DNA repair activity for these genes is indicated in the table. Increased HR gene expression is known to positively correlate with improved response to platinum based chemotherapy (a surrogate of HR deficiency) and thus can be predictive of decreased HR activity^{31,38}. Conceptually, a state of HR deficiency may lead to compensatory increased expression of other HR genes. **k,** Top-ranked Gene Ontology (GO) terms for the molecular functions encoded by the top 20 DNA repair genes defined in Extended Data Fig. 1g. **l,** Schematic representation of Pol0 domain structure with the helicases (BLM, RECQL4, RAD54B and RAD54L) that co-expressed with Pol0 (from Extended Data Fig. 1g). Conserved amino-acid sequences of ATP binding and hydrolysis motifs (namely Walker A and B) are indicated. Cox plots in **c** show twenty-fifth to seventy-fifth percentiles, with lines indicating the median, and whiskers indicating the smallest and largest values. For **d** and **e** (top panels), each dot represents the expression value from one patient, brackets show mean \pm s.e.m.



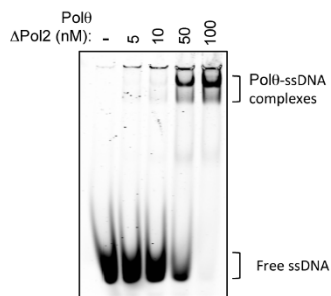
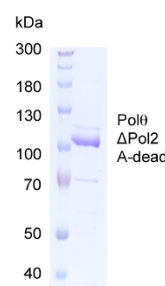
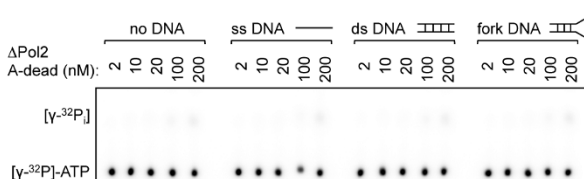
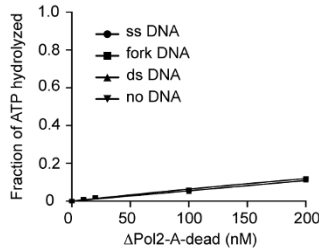
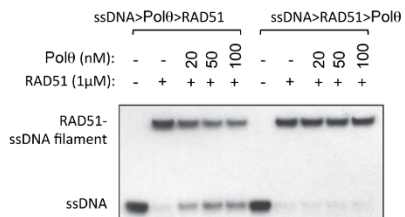
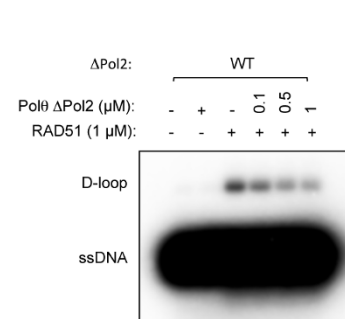
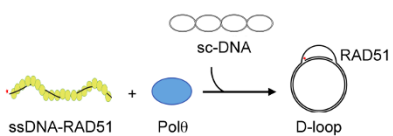
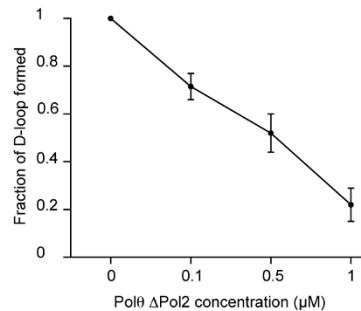
Extended Data Figure 2 | PoL0 is a RAD51-interacting protein required for maintenance of genomic stability. **a**, siRNA sequences (siPol01 and siPol02) efficiently downregulate exogenously transfected PoL0 protein. PoL0 levels were detected by immunoblotting with Flag or PoL0 antibody (left) and by RT-qPCR using 2 different sets of *POLQ* primers (right). The asterisk on the immunoblot indicates a non-specific band. Expression was normalized using *GAPDH* as a reference gene. *POLQ* gene expression values are displayed as fold-change differences relative to the mean expression in control cells, which was arbitrarily set to 1. **b**, Quantification of baseline and HU-induced RAD51 foci in U2OS cells transfected with the indicated siRNA. **c**, Quantification of baseline and HU-induced γH2AX foci in U2OS cells transfected with the indicated siRNA. **d**, Quantification of IR-induced RAD51 foci in BrdU-positive U2OS cells transfected with the indicated siRNA. **e**, PoL0 inhibition by siRNA induced a decrease in the cellular survival of 293T cells treated with MMC in a 3-day survival assay. **f**, Quantification of chromosomal aberrations in 293T cells transfected with the indicated siRNA. **g**, Schematic representation of PoL0 truncation proteins used for RAD51 interaction studies. **h**, Endogenous RAD51 co-precipitates with Flag-tagged PoL0-ΔPoL1 (PoL0-1-1416) but not PoL0-1633-Cter, each stably expressed in HeLa cells. **i**, Sequence alignment between the RAD51-interacting motifs of *C. elegans* RFS-1 and human PoL0. **j**, Schematic of PoL0 domain structure with its homologues HELQ and POLN. All data show mean \pm s.e.m.

indicated siRNA. **d**, Quantification of IR-induced RAD51 foci in BrdU-positive U2OS cells transfected with the indicated siRNA. **e**, PoL0 inhibition by siRNA induced a decrease in the cellular survival of 293T cells treated with MMC in a 3-day survival assay. **f**, Quantification of chromosomal aberrations in 293T cells transfected with the indicated siRNA. **g**, Schematic representation of PoL0 truncation proteins used for RAD51 interaction studies. **h**, Endogenous RAD51 co-precipitates with Flag-tagged PoL0-ΔPoL1 (PoL0-1-1416) but not PoL0-1633-Cter, each stably expressed in HeLa cells. **i**, Sequence alignment between the RAD51-interacting motifs of *C. elegans* RFS-1 and human PoL0. **j**, Schematic of PoL0 domain structure with its homologues HELQ and POLN. All data show mean \pm s.e.m.

a**b****c****d****e**

Extended Data Figure 3 | Characterization of RAD51-interacting motifs in Pol θ . **a**, Substitution peptide array probed with recombinant RAD51 and analysed by immunoblotting. A 20-mer peptide spanning each of the RAD51 binding sites (shown in Fig. 1g) were created in which each amino acid of the original peptide was mutated to each of the 20 amino acids and RAD51 binding activity was tested. The amino acid change for each of the amino acids of the RAD51 interacting domain of Pol θ is shown on the right. Ponceau staining was used to visualize position of the peptides within the array. **b**, GST-RAD51 pull-down with *in vitro* translated Pol θ proteins missing

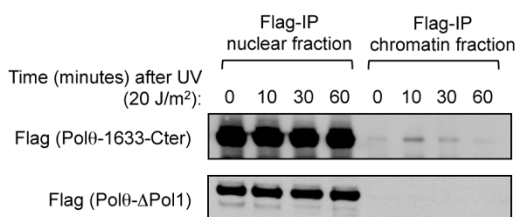
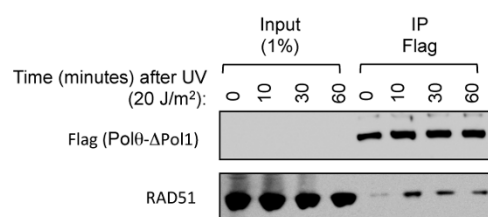
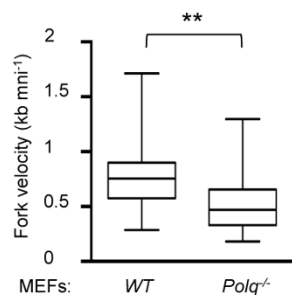
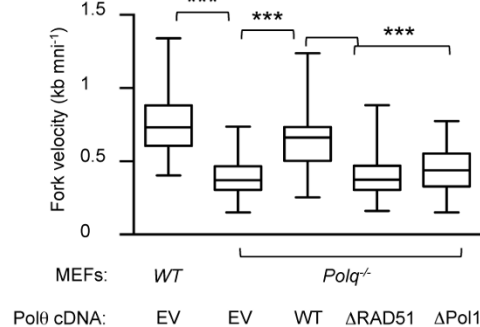
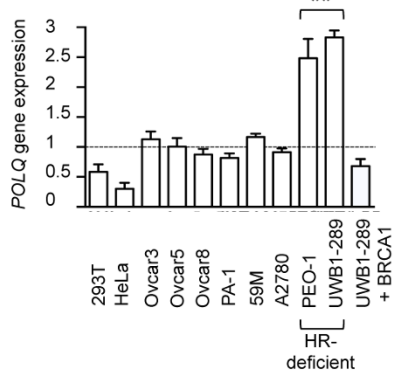
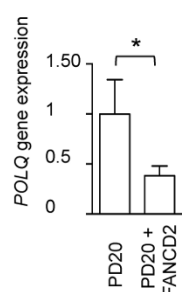
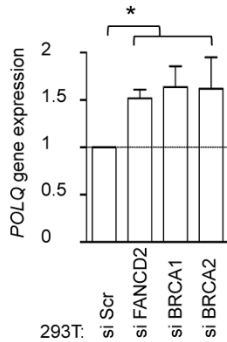
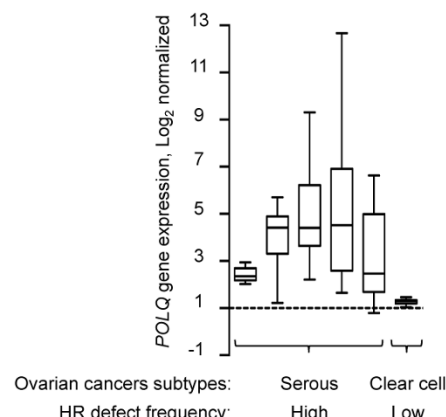
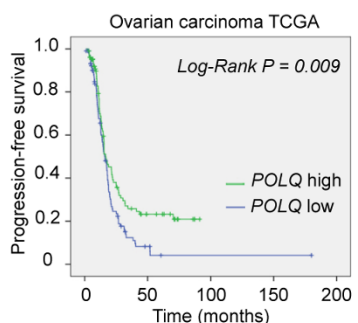
indicated amino acids. **c**, Schematic of Pol θ mutants used in complementation studies. **d**, Quantification of IR-induced RAD51 foci in U2OS cells stably integrated with empty vector (EV) or Pol θ - Δ Pol1 cDNA that is refractory to siPol θ . Cells were transfected with indicated siRNA and subsequently treated with IR. The number of cells with more than 10 RAD51 foci was calculated relative to control cells (si Scr). **e**, DR-GFP assay in U2OS cells stably integrated with empty vector (EV) or indicated Pol θ cDNA constructs refractory to siPol θ and transfected with indicated siRNA. All data show mean \pm s.e.m.

a**b****c****d****e****f****g****i****j**

Conditions tested	RAD51 foci	DR-GFP	RAD51-ssDNA assembly	D-loop formation
si Pol0	↑	↑	NA	NA
Pol0 cDNA WT	↓	↓	↓	↓
Pol0-A-dead cDNA	-	-	-	NA
Pol0-ΔRAD51 cDNA	-	-	-	NA

Extended Data Figure 4 | Pol0 is an ATPase that suppresses RAD51-ssDNA nucleofilament assembly and formation of RAD51-dependent D-loop structures. **a**, Representative ΔPol2 wild-type radiometric ATPase assay. **b**, Gel mobility shift assays with ΔPol2 wild type and ssDNA. **c**, Coomassie-stained gel showing the purified ΔPol2-A-dead fragment. **d**, Representative ΔPol2-A-dead radiometric ATPase assay. **e**, Quantification of ΔPol2-A-dead ATPase activity. (ssDNA, single-stranded DNA; dsDNA, double-stranded DNA). **f**, Assembly/disruption of RAD51-ssDNA filaments in the presence of

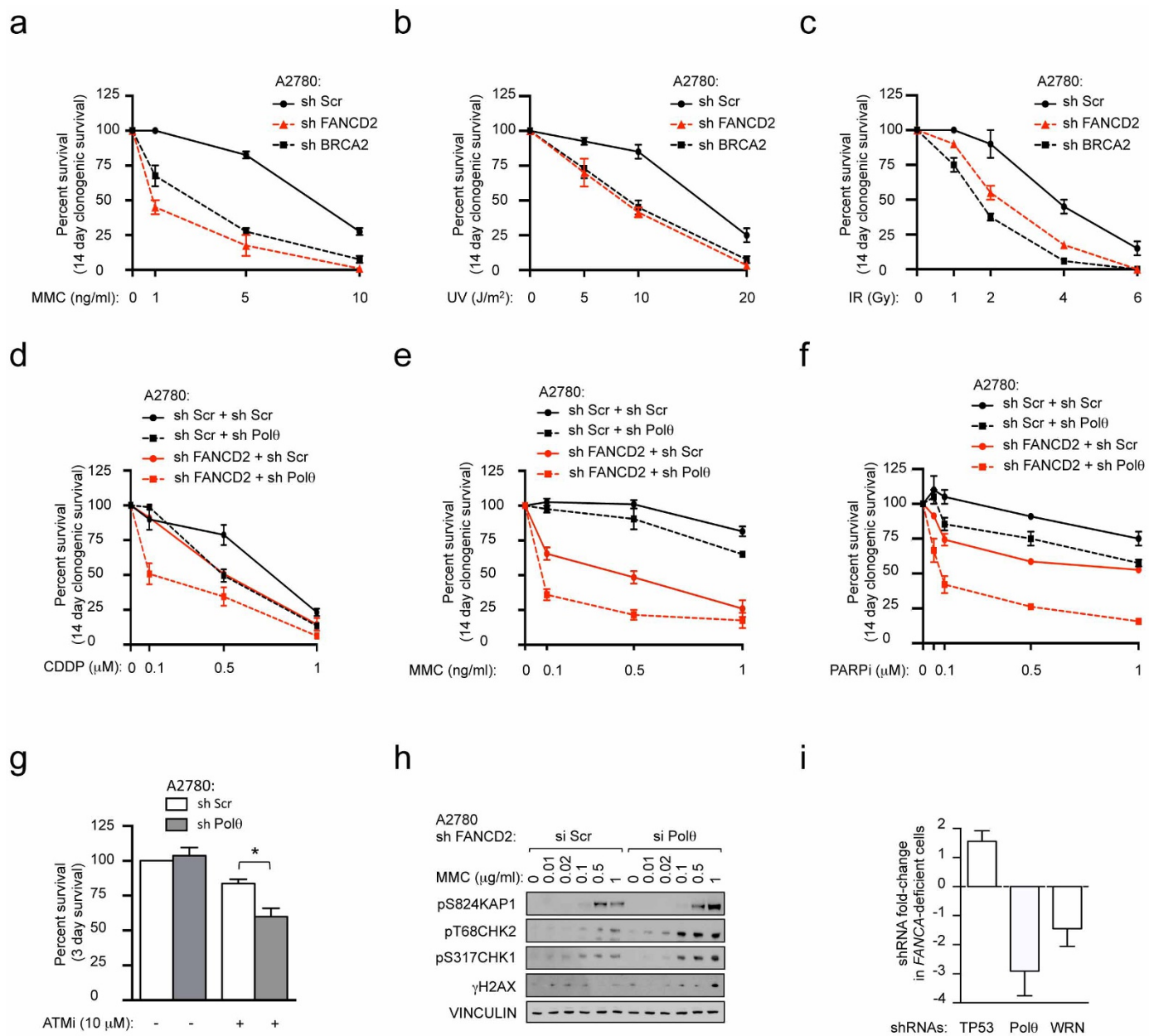
increasing amounts of ΔPol2 wild type. The order in which each component was added to the reaction is noted above. **g**, Schematics of the formation of RAD51-dependent D-loop structures. **h**, Formation of RAD51-containing D-loop structures following the addition of increasing amounts of ΔPol2 wild type. **i**, Fraction of D-loop formed following the addition of increasing amounts of ΔPol2 wild type. **j**, Effect of siPol0 and the different Pol0 cDNA constructs on HR read-out. NA, not applicable. Data in **i** shows mean \pm s.e.m.

a**b****c****d****e****f****g****h****i**

	POLQ expression	HR activity	Tumors sensitivity to CDDP or PARPi
Validated experimentally	-	+	-
	+	-	++
Hypothetical based	-	-	++++
	+	NA	++

Extended Data Figure 5 | Polθ functions under replicative stress and is induced by HR deficiency. **a**, Polθ recruitment to the chromatin is enhanced by UV treatment. HeLa cells stably integrated with either Flag-tagged ΔPol1 or Polθ-1633-Cter (Extended Data Fig. 2g) were subjected to UV treatment. Cells were collected at indicated time points after UV treatment and IPs were performed on nuclear and chromatin fractions. **b**, HeLa cells stably integrated with ΔPol1 were treated with UV and collected at the indicated time points following UV exposure. Polθ and RAD51 co-precipitation is enhanced by UV treatment. **c**, Quantification of DNA fibre lengths isolated from wild-type or *Polq*^{-/-} MEFs. **d**, Quantification of DNA fibre lengths isolated from wild-type or *Polq*^{-/-} MEFs transfected with either EV or Polθ cDNA constructs. **e**, *POLQ* gene expression was analysed by RT-qPCR in HR-deficient ovarian cancer cell lines (PEO-1 and UWB1-289) compared with other ovarian cancer cell lines, HeLa (cervical cancer) cells and 293T (transformed human embryonic kidney) cells. Expression was normalized using *GAPDH* gene as a reference. *POLQ* expression values are displayed as fold-change relative to the mean expression in HR-proficient control cells, which was arbitrarily set to 1. **f**, *POLQ* gene expression analysis (RT-qPCR) in 293T cells transfected with siRNA

targeting *FANCD2*, *BRCA1* or *BRCA2* (left panel) and in corrected PD20 cells (PD20 + FANCD2) relative to FANCD2-deficient cells (PD20) (right panel). Expression was normalized using *GAPDH* gene as a reference. *POLQ* expression values are presented as fold-change relative to the mean expression in control cells, which was arbitrarily set to 1. **g**, *POLQ* gene expression in 5 data sets of serous epithelial ovarian carcinoma (frequently associated with an HR deficiency) and 1 data set of clear cell ovarian carcinoma (subgroup not associated with HR alterations). For each data set, *POLQ* expression values are displayed as fold-change differences relative to the mean expression in control samples, which was arbitrarily set to 1. **h**, Progression-free survival (PFS) after first line platinum chemotherapy for patients with ovarian carcinoma (ovarian carcinoma TCGA). Statistical significance was assessed by the log-rank test ($P < 10^{-2}$). **i**, Effect of Polθ expression levels and HR status on tumour sensitivity to cisplatin or PARPi. NA, not applicable. Box plots in **c**, **d**, and **g** show twenty-fifth to seventy-fifth percentiles, with lines indicating the median, and whiskers indicating the smallest and largest values. Data in **e** and **f** show mean \pm s.e.m.

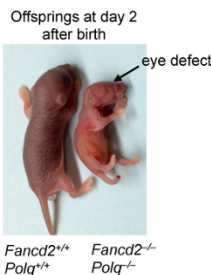


Extended Data Figure 6 | Pol0 inhibition sensitizes HR-deficient tumours to cytotoxic drug exposure. **a–c**, Clonogenic formation of A2780 cells expressing scrambled (Scr) shRNA or shRNAs against FANCD2 or BRCA2 with increasing amounts of MMC (**a**), UV (**b**) or IR (**c**). **d–f**, Clonogenic formation of A2780 cells expressing scrambled (Scr) or FANCD2 shRNA, together with shRNA targeting Pol0, in increasing concentrations of CDDP (**d**), MMC (**e**) or PARPi (**f**). **g**, Inhibition of Pol0 reduces the survival of A2780 cells after 3 days of continuous exposure to the ATM inhibitor Ku55933. **h**, Immunoblot analyses in A2780 cells expressing FANCD2 shRNA

together with siRNA targeting Pol0 or Scr at 24 h after indicated MMC pulse treatment. **i**, FANCA-deficient fibroblasts (GM6418) were infected with a whole-genome shRNA library and treated with MMC for 7 days. The fold-change enrichment of each shRNA after MMC treatment was determined by sequencing relative to the infected cells before treatment. TP53 depletion is known to improve survival of *FANCA*^{-/-} cells³³. WRN depletion has recently been shown to be synthetically lethal with HR deficiency³⁹. Each column represents the mean of at least 2 independent shRNAs. All data show mean ± s.e.m.

a

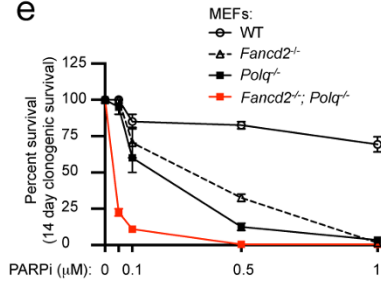
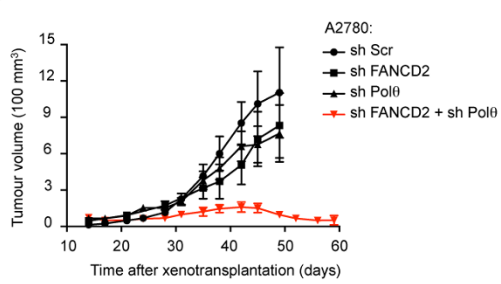
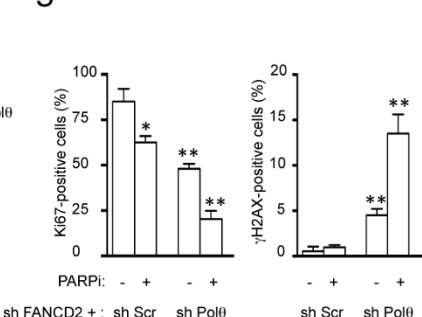
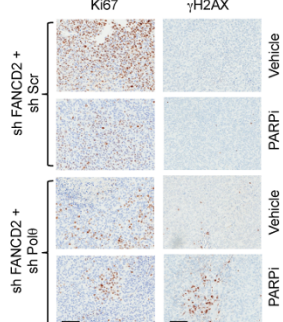
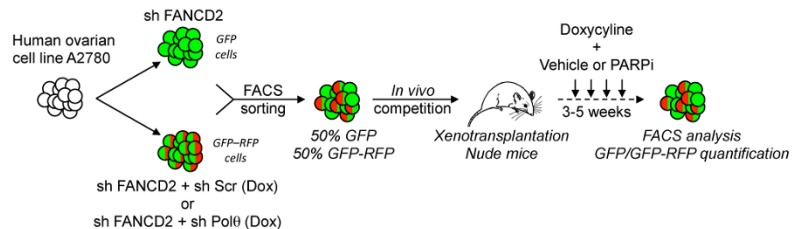
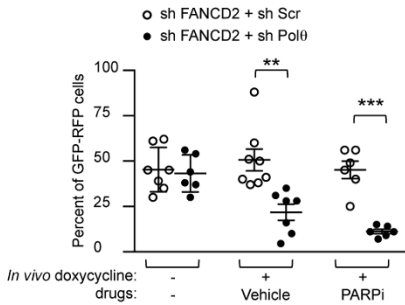
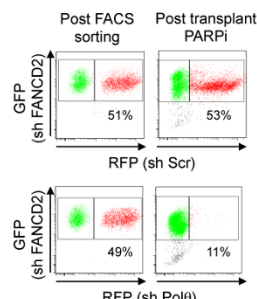
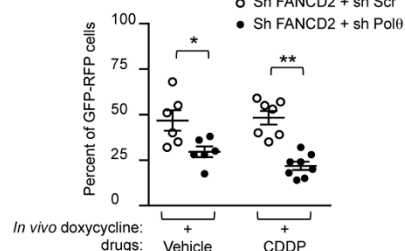
<i>Polq</i> status	<i>Fancd2</i> status	Offspring observed (n)	% observed	% expected	Significant difference
+/-	+/-	19	7.2	6.25	no
+/-	-/-	43	16.2	12.5	no
+/-	-/-	22	8.3	6.25	no
+/-	+/-	36	13.6	12.5	no
+/-	+/-	61	23.0	25	no
+/-	-/-	25	9.4	12.5	no
-/-	+/-	21	7.9	6.25	no
-/-	+/-	34	12.8	12.5	no
-/-	-/-	0 ^a	0	6.25	yes, $P < 0.001$
Total number :		261	100	100	

b**c**

<i>Polq</i> status	<i>Fancd2</i> status	Embryos observed (n)	% observed	% expected	Significant difference
+/-	+/-	13	6.6	6.25	no
+/-	-/-	31	15.7	12.5	no
+/-	-/-	7	3.6	6.25	no
+/-	+/-	22	11.2	12.5	no
+/-	+/-	62	31.5	25	no
+/-	-/-	28	14.2	12.5	no
-/-	+/-	10	5.1	6.25	no
-/-	+/-	16	8.1	12.5	no
-/-	-/-	8	4.1	6.25	no
Total number :		197	100	100	

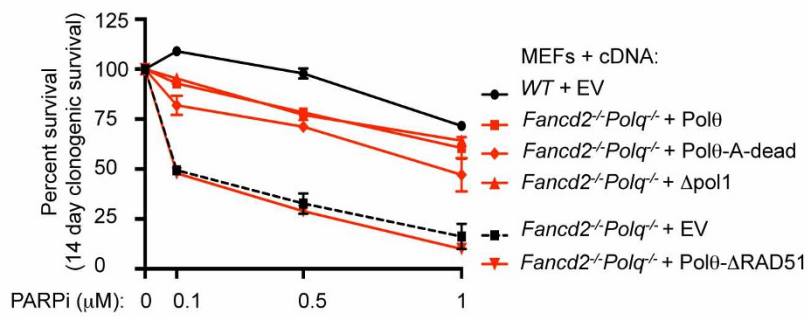
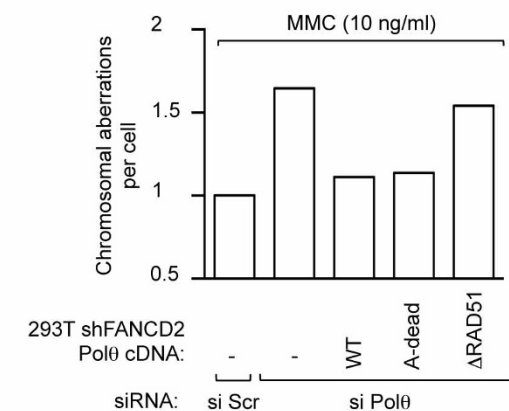
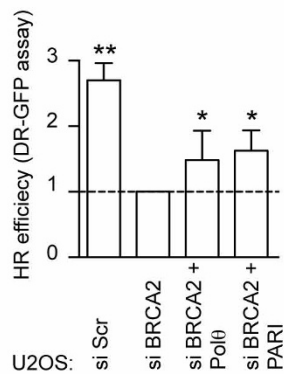
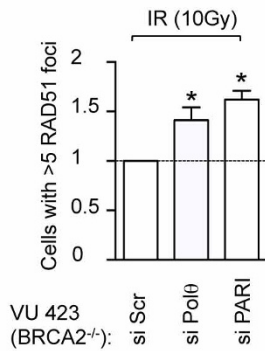
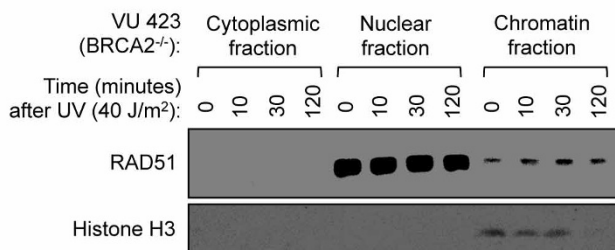
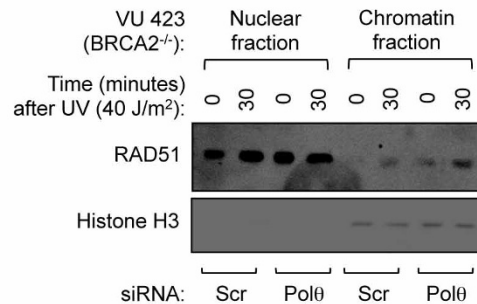
d

Malformation observed	% of <i>Polq</i> ^{-/-} <i>Fancd2</i> ^{-/-} embryos observed with malformations
Reduced body weight	100
Reduced body size	100
Eye defect	100
Limb malformation	12.5

e**f****g****h****i****j****k****l**

Extended Data Figure 7 | HR and Polθ repair pathways are synthetical lethal *in vivo*. **a**, Genotypes frequencies of offspring from interbred *Fancd2*^{+/−}/*Polq*^{+/−} mice. **Ψ**, four *Fancd2*^{−/−}/*Polq*^{−/−} offsprings were observed with several congenital malformations and premature death within 48 h of birth. **b**, Description of *Fancd2*^{−/−}/*Polq*^{−/−} offspring generated in the study. The offspring presented congenital malformations (that is, eye defects) together with reduced size and body weight. The arrow indicates absence of the right eye. **c**, Genotypes frequencies of E13.5 to E15 embryos (13.5 to 15 days post coitum) from interbred *Fancd2*^{+/−}/*Polq*^{+/−} mice. **d**, Description of congenital malformations and their measured frequencies observed in E13.5 to E15 *Fancd2*^{−/−}/*Polq*^{−/−} embryos generated in the study. **e**, Clonogenic formation of wild-type, *Fancd2*^{−/−}, *Polq*^{−/−} and *Fancd2*^{−/−}/*Polq*^{−/−} MEFs with increasing concentrations of PARPi. **f**, A2780 cells were transduced with indicated shRNAs and xenotransplanted into both flanks of athymic nude mice. The tumour volumes for individual mice were measured biweekly for 8 weeks.

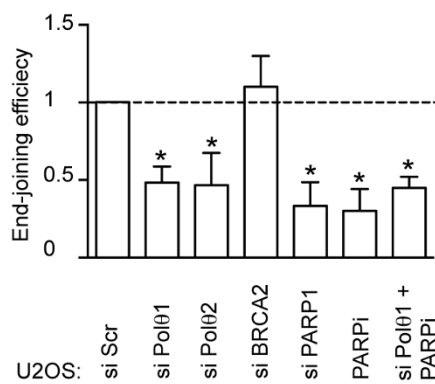
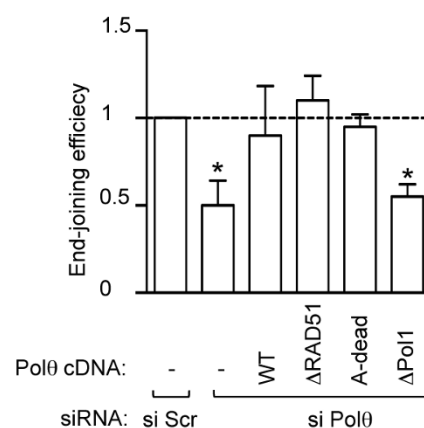
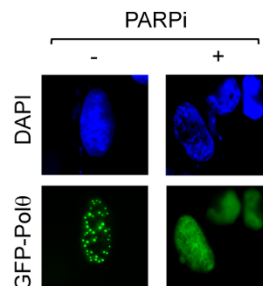
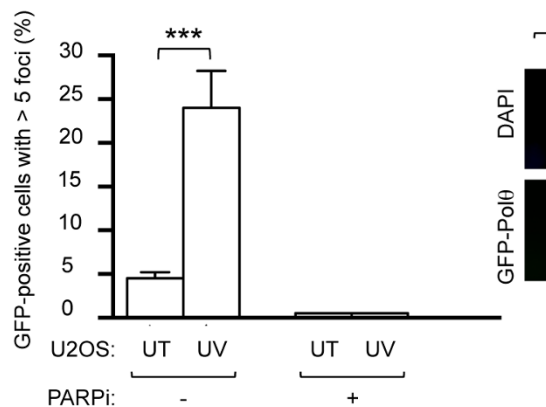
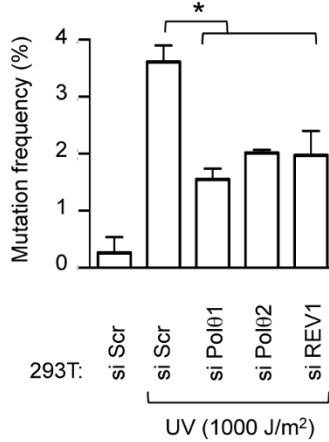
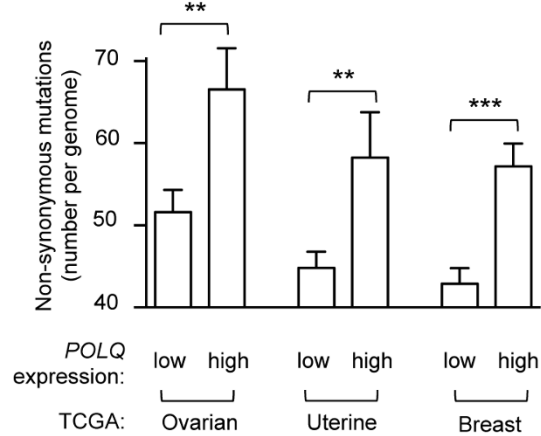
Each group represents $n \geq 5$ tumours from $n \geq 5$ mice. **g**, Ki67 and γ H2AX quantification in tumours treated with either vehicle or PARPi. **h**, Representative Ki67 and γ H2AX staining of A2780-shFANCD2 xenografts expressing sh Scr or sh Polθ in athymic nude mice, treated with either vehicle or PARPi. Scale bars, 100 μ M. **i**, *In vivo* competition assay design. **j**, Tumour chimaerism post-xenotransplantation for indicated conditions. **k**, Representative flow cytometry analysis of tumours before xenotransplantation (post-FACS sorting) or after xenotransplantation (post-transplant, PARPi). The percentage of GFP-RFP positive cells is indicated. **l**, Tumour chimaerism post-xenotransplantation for indicated conditions. For data in **j** and **l**, each circle represents data from one tumour and each group represents $n \geq 7$ tumours from $n \geq 6$ mice. Brackets show mean \pm s.e.m. Data in **e–g** show mean \pm s.e.m. For **f** each group represents $n \geq 6$ tumours from $n \geq 6$ mice.

a**b****c****d****e****f**

Extended Data Figure 8 | Polθ is required for HR-deficient cell survival and limits the formation of RAD51 structures in HR-deficient cells.

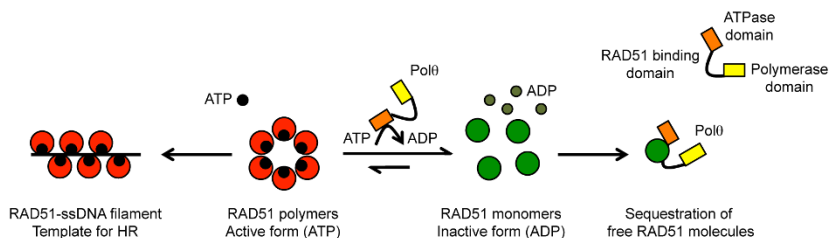
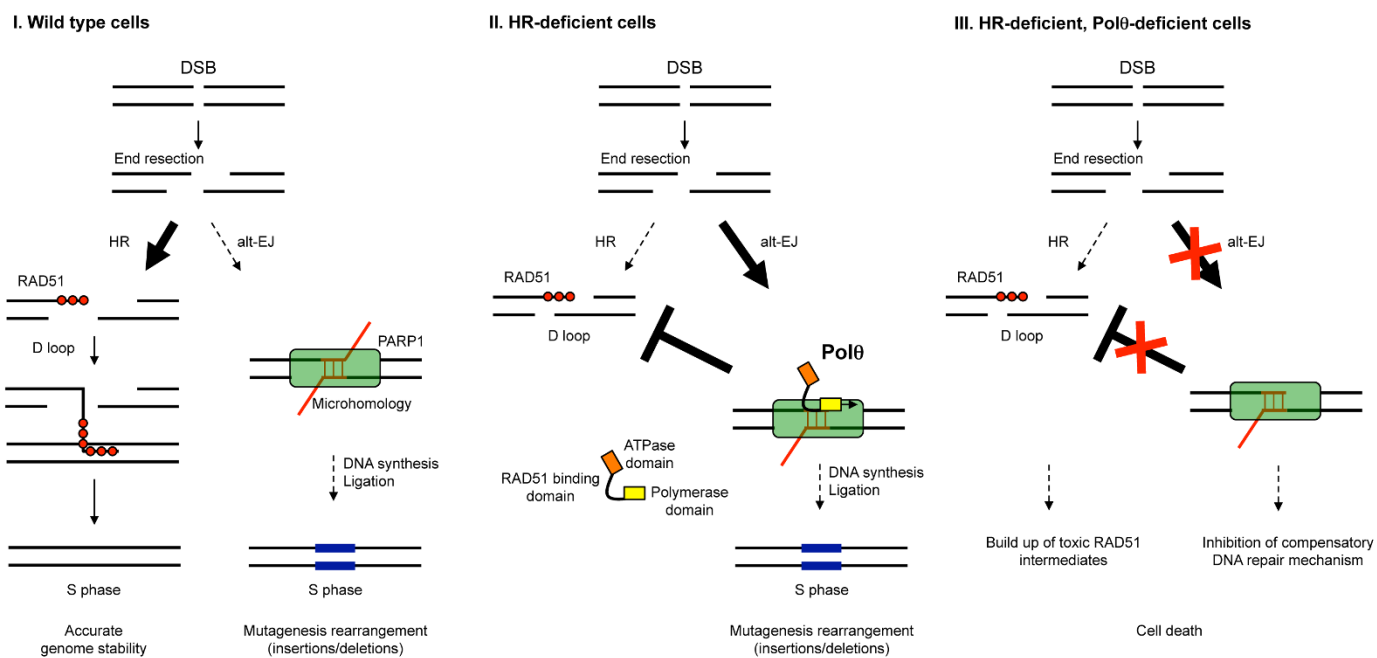
a, Clonogenic formation of *Fancd2^{-/-}Polq^{-/-}* MEFs transfected with full-length *POLQ* cDNA constructs in the presence of increasing concentrations of PARPi. **b**, Chromosome breakage analysis of FANCD2-depleted cells that were first transfected with the indicated siRNA and full-length *POLQ* cDNA constructs refractory to siPolθ and then exposed to MMC. **c**, DR-GFP assay in U2OS cells transfected with indicated siRNA. **d**, Quantification of baseline and

IR-induced RAD51 foci in U2OS cells transfected with indicated siRNA. **e**, RAD51 recruitment to chromatin is enhanced by UV treatment. VU 423 cells (*BRCA2^{-/-}*) were collected at indicated time points after UV treatment and immunoblotting performed on the cytoplasmic, nuclear and chromatin fractions. **f**, RAD51 recruitment to chromatin in VU 423 cells (*BRCA2^{-/-}*) transfected with indicated siRNA. Histone H3 was used as a control for chromatin fractionation. All data show mean \pm s.e.m.

a**b****c****d****e**

Extended Data Figure 9 | Pol0 participates in error-prone DNA repair.
a, End-joining reporter assay in U2OS cells transfected with indicated siRNA and/or treated with PARPi. **b**, End-joining reporter assay in U2OS cells transfected with indicated siRNA and *POLQ* cDNA constructs refractory to siPol01. **c**, UV damage-induced Pol0 foci formation in U2OS cells. Pol0 foci

were abolished by pre-treatment with PARPi. UT, untreated. **d**, Mutation frequency was determined in damaged supF plasmid, recovered from siRNA-treated 293T cells. **e**, Non-synonymous mutation count in ovarian, uterine and breast TCGA. All data show mean \pm s.e.m.

a**b**

Extended Data Figure 10 | Model depicting the role of Pol0 in DNA repair.
a, Mechanistic model for how Pol0 limits RAD51-ssDNA filament assembly. According to this model, the ATPase domain of Pol0 may prevent the assembly of RAD51 monomers into RAD51 polymers, perhaps by depleting local ATP concentrations. The RAD51 binding domains in the central region of Pol0 may then sequester the RAD51 monomers, preventing filament assembly.

b, (I) Under physiological conditions, Pol0 expression is low and its impact on repair of DNA double-strand breaks (DSB) is limited. (II) When HR deficiency occurs, Pol0 is then highly expressed and channels DSB repair towards alt-EJ. (III) In the case of an HR-defect, the loss of Pol0 leads to cell death through the persistence of toxic RAD51 intermediates and inhibition of alt-EJ.